Published for SISSA by Springer

Received: October 12, 2025
Accepted: March 24, 2026
Published: June 1, 2026

Search for dark matter production in association with bottom quarks and a lepton pair in proton-proton collisions at $\sqrt{s} = 13$ TeV

The CMS collaboration

Full author list at the end of the paper

E-mail: cms-publication-committee-chair@cern.ch

Abstract: A search is performed for dark matter produced in association with bottom quarks and a pair of electrons or muons in data collected with the CMS detector at the LHC, corresponding to 138 fb^{-1} of integrated luminosity of proton-proton collisions at a center-of-mass energy of 13 TeV. For the first time at the LHC, the associated production of a bottom quark-antiquark pair and a new heavy neutral Higgs boson (H) that subsequently decays into a leptonically decaying Z boson and a pseudoscalar (a) is explored. The latter acts as a dark matter mediator in the context of the two Higgs doublet model plus a pseudoscalar (2HDM+a). Multivariate techniques that target a wide range of mass configurations for the H and a particles are used. The observations are consistent with the expectations from standard model processes. Upper limits at 95% confidence level are set on the product of cross section and branching fraction of the new particles, ranging from 10^{-2} pb for an H mass of 400 GeV to 10^{-3} pb for an H mass of 2000 GeV. Constraints on the parameter space of a benchmark 2HDM+a model are derived and compared with expectations in the context of cosmological predictions.

Keywords: Beyond Standard Model, Dark Matter, Hadron-Hadron Scattering

ArXiv ePrint: 2510.12396

https://doi.org/10.1007/JHEP06(2026)014

JHEP06(2026)014

Contents

1 Introduction 1

2 The CMS detector 3

3 Data and simulated samples 4

4 Event reconstruction 6

5 Event selection 7
- 5.1 Baseline selection 7
- 5.2 Signal region selection 8
- 5.3 Multivariate optimization 9

6 Background estimation 10

7 Systematic uncertainties 13

8 Results 17
- 8.1 Upper limits on the signal cross sections 20
- 8.2 Interpretation in the 2HDM+a context 20

9 Summary 23

The CMS collaboration 32

JHEP06(2026)014

1 Introduction

The nature of dark matter (DM) is unknown. A prevalent hypothesis suggests that the DM could exist in the form of a weakly interacting massive particle (WIMP) [1, 2]. Many WIMP candidates, hereafter referred to simply as "DM particles", are expected to have been thermally produced in the early universe, similar to the particles of the standard model (SM). If the mass of the DM particle is in the GeV-TeV range, the respective relic abundance can be obtained via thermal freeze-out in the early universe [3, 4].

An extensive experimental program is currently ongoing to search for DM particles through interactions with SM particles. Three main approaches broadly cover the efforts of DM detection: direct searches, indirect searches, and searches at colliders. Direct searches aim at detecting the scattering of ambient DM particles from nuclei, while in indirect searches the energetic particles possibly produced by DM annihilations in space are analyzed. Complementary to these two approaches, searches for the production of DM particles at particle colliders created under well-controlled conditions are also of high relevance. Since DM particles would escape detection, their presence would lead to events involving an imbalance in the vector sum of the measured transverse momenta through the presence of missing

transverse momentum ($p_{\mathrm{T}}^{\mathrm{miss}}$) recoiling against a visible final state X. Searches for events with large $p_{\mathrm{T}}^{\mathrm{miss}}$ are currently a major focus at CERN's LHC [5–8].

Recently, the Fermi-LAT space telescope observed a gamma-ray excess in studies of the Milky Way galactic center [9]. While the consistency with other observations in astroparticle physics and cosmology is still under discussion [10], this might be interpreted as the existence of weak-scale DM annihilating into bottom quark-antiquark ($\mathrm{b\overline{b}}$) pairs [11–14]. A compelling interpretation of the gamma-ray excess from the galactic center, in agreement with the fact that no DM particle has been observed in direct detection experiments so far, is given by the existence of a pseudoscalar mediator between the SM and DM sectors [15–17]. This would lead to spin-dependent DM-nucleon interactions, for which experimental limits are much less stringent than for spin-independent interactions [18–21]. In general, the strength of DM-nucleon interactions mediated by pseudoscalars is below the reach of present direct DM detection experiments [22, 23].

In this paper, we present a novel DM search for events involving final states with a $\mathrm{b\overline{b}}$ pair, a leptonically decaying Z boson, and $p_{\mathrm{T}}^{\mathrm{miss}}$. The search is performed using data recorded with the CMS detector at the LHC in proton-proton (pp) collisions at a center-of-mass energy of 13 TeV. Such a signature could be produced in scenarios beyond the SM (BSM) with a pseudoscalar providing the link between visible SM particles and the dark sector. This signature is particularly interesting as it might be sensitive to unexplored regions of the parameter space where searches for DM [24–40] and flavor bounds [41–47] can not reach. Additionally, it can serve as a test of the DM interpretation of the gamma-ray galactic center excess [3].

One alternative to generate a gauge-invariant and renormalizable model featuring a pseudoscalar DM mediator is to introduce an additional Higgs doublet, as typically done in the so-called two Higgs doublet models (2HDMs) [48–51]. In this scenario, the coupling of a DM mediator to SM fermions is naturally generated by introducing a new pseudoscalar field that mixes with the 2HDM pseudoscalar field. This new field couples directly to the DM candidate, thus naturally providing a connection between the SM and DM sectors. The resulting model is referred to as 2HDM+a [52], and has been thoroughly studied in the context of the LHC Dark Matter Working Group [53]. The scalar sector of the 2HDM+a contains a charged scalar $\mathrm{H}^{\pm}$, two neutral 2HDM CP-even scalars H and h, and two neutral 2HDM CP-odd scalars A and a. The mixing between the pseudoscalar components allows both A and a to couple simultaneously to DM and SM fermions, providing the portal between the visible and DM sectors. The angle that controls this mixing is called θ. The ratio of the vacuum expectation values of the two doublets is given by $\tan\beta$, while the mixing angle α in the neutral CP-even sector satisfies $\beta - \alpha = \pi/2$.

An additional incentive to further examine the 2HDM+a is that this theoretical construction is able to correctly predict the DM relic density when DM is annihilated via an s-channel process into SM fermions. When the mass of the DM particles is chosen to match the mass range preferred by the gamma-ray excess, the observed DM relic density tends to favor relatively large values of $\tan\beta$ [3]. Larger values of this parameter lead to larger couplings of the heavy scalar states to down-type fermions, such as bottom quarks. This configuration motivates the search channel investigated in this paper, namely heavy

JHEP06(2026)014

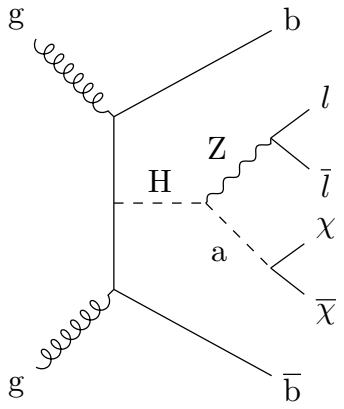

Figure 1. Example diagram at leading order for the production of a heavy pseudoscalar mediator decaying into dark matter particles, in association with $Z(\rightarrow l\bar{l})b\bar{b}$.

H production in association with a $b\bar{b}$ pair ($b\bar{b}H$), where the heavy scalar and the new pseudoscalar particles decay as $H \rightarrow Za \rightarrow (l\bar{l})(\chi\bar{\chi})$ in which l denotes an electron (e), a muon (μ), or a tau (τ) lepton and χ and $\bar{\chi}$ a DM particle and antiparticle, respectively. Although l can also be a τ lepton, the analysis only focuses on final states with a pair of electrons or muons. An example diagram for the process described above is shown in figure 1. Searching for this process at the LHC allows probing the region of parameter space consistent with a DM interpretation of the gamma-ray galactic center excess, not accessible through other processes. For example, ref. [3] demonstrates that this channel provides feasible access to the intermediate $\tan\beta$ region ($\tan\beta \approx 10$), while simultaneously probing mixing values down to $\sin\theta \approx 0.1$. In this article, we present the first dedicated experimental analysis of this channel in the context of searches for DM at colliders.

This article is organized as follows. After a brief description of the CMS detector in section 2, the data and simulated samples are described in section 3. In section 4, the event reconstruction is outlined, while section 5 describes the event selection, including the multivariate analysis. The background estimation is discussed in section 6, while the systematic uncertainties are given in section 7. The final results are presented in section 8 and a summary is given in section 9. Tabulated results are provided in the HEPData record for this analysis [54].

2 The CMS detector

The central feature of the CMS apparatus is a superconducting solenoid of 6 m internal diameter, providing a magnetic field of 3.8 T. Within the solenoid volume are a silicon pixel and strip tracker, a lead tungstate crystal electromagnetic calorimeter (ECAL), and a brass and scintillator hadron calorimeter (HCAL), each composed of a barrel and two endcap sections. Forward calorimeters extend the pseudorapidity (η) coverage provided by the barrel and endcap detectors. Muons are measured in gas-ionization detectors embedded in the steel flux-return yoke outside the solenoid. More detailed descriptions of the CMS detector, together with a definition of the coordinate system used and the relevant kinematic variables, can be found in ref. [55].

JHEP06(2026)014

Events of interest are selected using a two-tiered trigger system. The first level, composed of custom hardware processors, uses information from the calorimeters and muon detectors to select events at a rate of around 100 kHz within a fixed latency of 4 μs [56]. The second level, known as the high-level trigger, consists of a farm of processors running a version of the full event reconstruction software optimized for fast processing, and reduces the event rate to around 1 kHz before data storage [57].

3 Data and simulated samples

This search uses data recorded in 2016–2018 with the CMS detector, corresponding to an integrated luminosity of 138 fb^{-1}. The data sets used in the analysis have been selected by a lepton trigger, which is composed of a combined logical OR of single-lepton and dilepton triggers. The dilepton triggers have isolation requirements and transverse momentum (p_{T}) thresholds of 17–23 and 8–12 GeV for the leading and subleading leptons, respectively. The inclusion of single-lepton triggers with lepton p_{T} threshold higher than 23 GeV and no isolation requirement is important to select signal events with two energetic leptons spatially close to each other that occur more frequently as $m_{\mathrm{H}} - m_{\mathrm{a}}$ increases. This results in high trigger efficiency compared to isolated lepton triggers when the leptons are reconstructed in each other's isolation cones. The lepton trigger efficiencies are measured in data and simulation using independent triggers based on $p_{\mathrm{T}}^{\mathrm{miss}}$. The average trigger efficiency, evaluated across lepton p_{T} and η bins, is 98.6%. Correction factors are derived and applied to the simulated samples to match the trigger efficiencies measured in the data.

The signal process is simulated at leading order (LO) using MadGraph5_aMC@NLO (MG5) v2.6.5 [58] with a dedicated 2HDM+a model [52]. The benchmark scenario investigated is summarized as

$$\begin{aligned} m_{\mathrm{H}} = m_{\mathrm{A}} = m_{\mathrm{H}^{\pm}}, \qquad & m_{\mathrm{h}} = 125\,\mathrm{GeV}, \quad m_{\chi} = 45\,\mathrm{GeV}, \\ \cos(\beta-\alpha) = 0, \qquad & \tan\beta = 11, \qquad \sin\theta = 0.35, \\ \lambda_3 = \lambda_{P_1} = \lambda_{P_2} = 0.25, \quad & \text{and} \quad y_{\chi} = 1, \end{aligned} \tag{3.1}$$

where m_{H}, m_{A}, and $m_{\mathrm{H}^{\pm}}$ are the masses of heavy Higgs bosons, while the light neutral CP-even scalar h is identified with the Higgs boson. The mass of the pseudoscalar mediator and the DM particle are denoted with m_{a} and m_{χ}, respectively. The λ_{P_1} and λ_{P_2} parameters control the quartic interactions between the doublets and the singlet, λ_3 mediates the same quartic interaction but only between the two doublets, and y_{χ} is the parameter that controls the strength of the interaction between the singlet scalar and the DM fermion χ. The couplings of A and a to DM particles are given by $y_{\chi}\cos\theta$ and $y_{\chi}\sin\theta$, respectively. A thorough study of various constraints implied by the parameter choices of eq. (3.1) is presented in ref. [53]. The value of m_{χ} is chosen according to refs. [3, 14], where it is shown that such a value lies close to the preferred range ($m_{\chi} \in [50, 170]$ GeV) of the gamma-ray galactic-center excess if DM annihilates into $\mathrm{b\bar{b}}$. Its exact value is irrelevant for this search when it is below half the mass of the mediator. Different signal samples are generated for the scalar masses m_{H} and m_{a}, taken as free parameters, with $m_{\mathrm{H}} (> m_{\mathrm{a}} + m_{\mathrm{Z}})$ between 400 and 2000 GeV and $m_{\mathrm{a}} (> 2m_{\chi})$ between 100 and 1800 GeV. The λ_3 parameter is set to $\lambda_3 = m_{\mathrm{h}}^2/v^2 \approx 0.25$, with

JHEP06(2026)014

v the electroweak vacuum expectation value. In this configuration, the contribution from the $H \to aa$ channel becomes insignificant, as shown in ref. [52], thus guaranteeing a sufficiently narrow width of the heavy scalar resonance. The H boson width has been calculated for relevant variations of the other 2HDM+a parameters for this analysis, verifying the validity of the narrow-width approximation for both new resonances.

The SM processes with the largest contributions to the background in this analysis are Drell-Yan (DY) $Z/\gamma^* \to l\bar{l}$, top quark-antiquark pair ($t\bar{t}$), single top quark, and diboson (in particular WZ and ZZ) production. For the ZZ case, if one of the Z bosons decays to a charged lepton pair while the other decays to a pair of neutrinos, this results in an irreducible signature if an initial-state radiation jet is identified as b jet. Similarly for the WZ process, if the charged lepton from the W boson decay is lost or not identified, this can result in a signal-like signature.

Samples of $Z/\gamma^* \to l\bar{l}$ events are generated at next-to-leading order (NLO) in quantum chromodynamics (QCD) using MG5 with the FxFx prescription [59] for matching and merging of two additional jets from the matrix element (ME) calculation to the parton shower. Simulated events of $t\bar{t}$, single top quark production in the t channel and in association with a W boson (tW), WZ, and ZZ are generated at NLO in QCD using POWHEG v2 [60, 61]. Single top quark production in the s channel is simulated at NLO in QCD using MG5. Additional minor SM contributions from VV, VVV, $t\bar{t}V$, $t\bar{t}VV$, and tZq processes, in which V stands for W or Z, will be referred to as "Other" and are simulated with MG5 at NLO or LO in QCD, depending on the process.

All background samples are normalized using the most accurate cross section calculations available, which generally incorporate NLO or next-to-NLO (NNLO) precision [62–65]. It was also observed that the p_T spectra of top quarks in $t\bar{t}$ data were significantly softer than those predicted by simulations based on either LO or NLO matrix elements interfaced with parton showers. The simulation can be improved considering a correction based on the latest theoretical NNLO QCD + NLO electroweak (EW) calculation for the SM $t\bar{t}$ production [66]. The correction was implemented by a reweighting procedure with correction factors depending on the p_T of the top quark and antiquark. It is applied to the events of the NLO sample simulating the $t\bar{t}$ process. Similarly, for the WZ process, a correction based on NNLO QCD + NLO EW fixed-order predictions obtained using MATRIX v2.0.0.beta1 [67, 68] has been incorporated via reweighting the simulated WZ sample with correction factors depending on the p_T of the W boson. For all the above-described simulations, the initial-state partons are modeled with the NNPDF 3.1 NNLO [69] parton distribution functions (PDFs). Parton showering, hadronization, and the underlying event dynamics are handled by PYTHIA v8.240 [70] using the CP5 tune [71]. All signal and background samples are processed using GEANT4 [72] to provide a full simulation of the CMS detector, including a simulation of the triggers.

The effects of additional pp interactions in the same or adjacent bunch crossings, referred to as pileup, are included in all simulation samples. A reweighting procedure is used to match the simulated distribution of pileup interactions with the one observed in data.

JHEP06(2026)014

4 Event reconstruction

The particle-flow (PF) algorithm [73] aims to reconstruct and identify each individual particle in an event, with an optimized combination of information from the various elements of the CMS detector including charged particle tracks from the tracking detector, energy deposits in the HCAL and ECAL, and reconstructed tracks from the muon chambers. Particles in each event are reconstructed and identified as either electrons, muons, photons, charged hadrons, or neutral hadrons. The primary vertex is taken to be the vertex corresponding to the hardest scattering in the event, selected as the vertex with the highest quadratic sum of the p_{T} from all tracks associated with it [74].

Electrons are identified as a primary track and potentially multiple ECAL energy clusters corresponding to the extrapolation of this track to the ECAL and to possible bremsstrahlung photons emitted along the way. The energy of electrons is deduced from the electron momentum at the PV, as determined by the tracker, the energy of the corresponding ECAL cluster, and the cumulative energy from all bremsstrahlung photons which have their origin spatially compatible with the electron track. An identification algorithm [75] is applied using multivariate techniques and including isolation information during the training. A working point with an identification efficiency of 90% and a misidentification rate of 1% for jets misidentified as electrons is used. Only electrons with $p_{\mathrm{T}} > 20\,\mathrm{GeV}$, $|\eta| < 2.5$, and $|\eta_{\mathrm{SC}}| \notin [1.444, 1.566]$ are selected, where η_{SC} is the η of the ECAL cluster corresponding to the electron candidate. The η_{SC} requirement aims to avoid a gap between the ECAL barrel and endcap components. Corrections for electron reconstruction and identification efficiencies are applied to simulated events to improve the agreement between data and simulation [75].

Muons are identified as tracks in the tracker consistent with either a track or several hits in the muon system, and associated with calorimeter deposits compatible with the muon hypothesis. The momentum of muons is obtained from the curvature of the corresponding track. In this analysis, muons must be isolated from charged hadrons and neutral particles, and pass the "medium" identification criteria [76] optimized for prompt muons and muons from heavy flavor decay, having an identification efficiency of 98% and misidentification rates of pions and kaons as muons below 0.2% and 0.5%, respectively. Muons are required to have $p_{\mathrm{T}} > 20\,\mathrm{GeV}$ and $|\eta| < 2.4$. Corrections for muon reconstruction, identification, and isolation efficiencies are applied to simulated events to improve the agreement with data [76].

The PF candidates are clustered into jets using the anti-k_{T} clustering algorithm [77], with a distance parameter of 0.4, implemented in the FastJet package [78, 79]. Charged particles reconstructed from tracks associated with pileup vertices are omitted from the clustering to reduce the impact of pileup collisions, while charged particles associated with the primary vertex and all neutral particles are kept. The jet energy is determined from the vectorial sum of all particle four-momenta in the jet and is found from simulation to be, on average, within 5–10% of the true momentum over the entire p_{T} spectrum and detector acceptance. Jet energy corrections are derived from simulation studies so that the average measured energy of reconstructed jets becomes identical to that of particle-level jets. Measurements using dijet, photon+jet, Z+jet, and multijet events are used to determine any residual differences between the jet energy scale in data and simulation [80], and appropriate corrections are

JHEP06(2026)014

made. The energy resolution of simulated jets is also corrected to match the resolution in the data, and typically amounts to 15–20% at 30 GeV, 10% at 100 GeV, and 5% at 1 TeV [80].

Jets in the angular vicinity of a selected electron or muon with $\Delta R < 0.4$ are removed from the analysis, where $\Delta R = \sqrt{(\Delta\eta)^2 + (\Delta\phi)^2}$ with $\Delta\eta$ and $\Delta\phi$ as the distances in pseudorapidity and azimuth, respectively, between the lepton and the jet. Jets must have $p_T > 20$ GeV and $|\eta| < 2.4$ to be considered in this analysis. Jets with $p_T < 50$ GeV are required to pass the loose working point criteria of the pileup jet identification [81] to suppress jets from pileup interactions. The DeepCSV algorithm [82] is used to identify jets originating from the fragmentation of a b quark (b jets), at a loose working point defined by an inclusive light-quark or gluon jet misidentification rate of 10%, resulting in a b-jet identification efficiency of 84%. Additional corrections are applied to cover remaining residual differences between data and simulation that arise from pileup and b-tagged jet identification efficiencies.

The missing transverse momentum vector $\vec{p}_T^{\,\text{miss}}$ is computed for each event as the negative vector sum of the transverse momenta of the reconstructed physics objects, namely muons, electrons, photons, hadronically decaying τ leptons, jets, and unclustered energy [83]. The unclustered energy is the contribution from the PF candidates not associated with any of the previous physics objects. The $\vec{p}_T^{\,\text{miss}}$ is modified to account for corrections to the energy scale and resolution of reconstructed jets in the event. Its magnitude, denoted as p_T^{miss}, is an important observable in this analysis because it provides information related to the DM candidates in signal events. Collision events can exhibit unusually large values of p_T^{miss} which may be attributed to reconstruction failures, detector malfunctions, or noncollision backgrounds. To address these issues, filters are designed to detect and reject events with spurious p_T^{miss} values, having an efficiency of 85%–90% and a misidentification rate of less than 0.1% [83]. These filters are applied to data and simulated events.

5 Event selection

The signal topology in this analysis consists of a pair of leptons from a Z boson decay with opposite electrical charge and same flavor, the presence of b jets, and a substantial amount of p_T^{miss} from the $a \to \chi\bar{\chi}$ decay. The event selection starts with a sequence of requirements in kinematic variables referred to as baseline selection, which are applied in all regions defined in the analysis. Additional requirements are imposed to separate the remaining events into the signal region (SR) and control regions (CRs).

5.1 Baseline selection

The selection requires at least one jet and two opposite-sign (OS) leptons (ℓ_1 and ℓ_2) where only e^-e^+, $\mu^-\mu^+$, $e^-\mu^+$, and μ^-e^+ pairs are considered. If there are more than two leptons in an event, the chosen OS dilepton system is the one with the reconstructed invariant mass closer to m_Z, assumed to be 91.19 GeV [84]. The lepton with the highest p_T must have $p_T^{\ell_1} > 40$ GeV. The dilepton system must have transverse momentum $p_T^{\ell\ell} > 40$ GeV, an angular distance between the two leptons $\Delta R^{\ell\ell} < 3.2$, and a small mass difference $\Delta m^{\ell\ell} = |m_{\ell\ell} - m_Z| < 25$ GeV, intended to reduce the number of events from nonresonant sources. The requirement $p_T^{\text{miss}} > 65$ GeV removes SM backgrounds without high-p_T neutrinos

JHEP06(2026)014

in the final state. In signal events, the Z boson and the pseudoscalar particle are more likely to be emitted back-to-back in ϕ. The difference in azimuthal angle between the dilepton system and $\vec{p}_{\mathrm{T}}^{\,\mathrm{miss}}$ must satisfy $\Delta\phi^{\ell\ell,p_{\mathrm{T}}^{\mathrm{miss}}} > 0.8$. A quantity that is related to the mass of the heavy scalar is the transverse mass $m_{\mathrm{T}}^{\ell\ell,p_{\mathrm{T}}^{\mathrm{miss}}}$ of the system formed by the dilepton system and $\vec{p}_{\mathrm{T}}^{\,\mathrm{miss}}$ [85]. Events are required to have $m_{\mathrm{T}}^{\ell\ell,p_{\mathrm{T}}^{\mathrm{miss}}} > 90\,\mathrm{GeV}$.

The baseline selection removes more than 97% of the events from each of the main background processes. The impact on the signals is a reduction in selection efficiency by about 10% from the $N_{\mathrm{jets}} \geq 1$ requirement, and 3–8% from the other requirements depending on the signal sample.

5.2 Signal region selection

Because the two b quarks produced in signal events typically have low p_{T}, many of the corresponding jets do not pass the $p_{\mathrm{T}} > 20\,\mathrm{GeV}$ criterion applied at event reconstruction. To maximize the acceptance, only a loose b-jet requirement is adopted for the SR that consists of the presence of at least one b jet with the loose b tagging working point ($N_{\mathrm{b}} \geq 1$) defined in section 4. Additionally, the events must have exactly two opposite-sign same-flavor (OSSF) leptons ($\mathrm{e}^+\mathrm{e}^-$ or $\mu^+\mu^-$).

To suppress the contamination of $\mathrm{t\bar{t}}$ production in events with two reconstructed leptons and b jets, an analytical method is used to reconstruct and identify such events [86]. This method makes use of an algebraic approach to solve a system of equations with six kinematic constraints to determine the unknown momentum vectors of the two undetected neutrinos. The constraint equations are constructed using the four momenta of the two leptons, two jets, and $\vec{p}_{\mathrm{T}}^{\,\mathrm{miss}}$, assuming the top quark and W masses to be 172.5 and 80.37 GeV, respectively [84]. Events with an analytic solution to this set of equations are assumed to be from $\mathrm{t\bar{t}}$ production.

The $\mathrm{t\bar{t}}$ event reconstruction is performed on events with at least two jets and one b-tagged jet. If there are more than two jets in an event, the algorithm tries to find a solution as follows.

- In events with two or more b-tagged jets, all pairs of b-tagged jets are used in the reconstruction. If solutions exist, these are considered by the algorithm.
- If no solution is found in the previous hypothesis or if the event has only one b-tagged jet, all pairs of a b-tagged jet with another jet are used in the reconstruction. Again, if solutions exist, these are considered by the algorithm.

For any of the above cases, the generator level distributions of the neutrino energy (E_ν) and antineutrino energy ($E_{\bar{\nu}}$), as obtained from simulated $\mathrm{t\bar{t}}$ production, are used as probability distributions. The best solution is the one with the reconstructed values of E_ν and $E_{\bar{\nu}}$ associated with the highest probability. In case there is no solution, the event is considered to have not originated from $\mathrm{t\bar{t}}$ production.

The non-existence of an analytical solution for the $\mathrm{t\bar{t}}$ event reconstruction described above is added as the last requirement for the SR selection. By doing that, about 60% of the $\mathrm{t\bar{t}}$ dilepton events are removed from the SR, while reducing the signal efficiency by 0.2–5%, depending on the signal sample. A list of all requirements used to define the SR is given in table 1.

JHEP06(2026)014

Baseline selection	SR selection
Has two OS leptons	Pass baseline selection
$p_{\mathrm{T}}^{\ell_1} > 40\,\mathrm{GeV}$	$N_{\mathrm{b}} \geq 1$
$p_{\mathrm{T}}^{\mathrm{miss}} > 65\,\mathrm{GeV}$	$N_{\mathrm{leptons}} = 2$
$p_{\mathrm{T}}^{\ell\ell} > 40\,\mathrm{GeV}$	ℓ_1 and ℓ_2 are OSSF
$\Delta m^{\ell\ell} < 25\,\mathrm{GeV}$	No $\mathrm{t\bar{t}}$ analytic solution
$\Delta R^{\ell\ell} < 3.2$	
$\Delta\phi^{\ell\ell,p_{\mathrm{T}}^{\mathrm{miss}}} > 0.8$	
$m_{\mathrm{T}}^{\ell\ell,p_{\mathrm{T}}^{\mathrm{miss}}} > 90\,\mathrm{GeV}$	
$N_{\mathrm{jets}} \geq 1$	

Table 1. List of requirements used to define the SR, split into a baseline and an SR region selection.

The majority of ZZ events in the SR come from $\mathrm{ZZ} \to 2\ell 2\nu$, while for WZ events, the main channel is $\mathrm{WZ} \to 3\ell\nu$ with one lepton not reconstructed. Except for $\mathrm{ZZ} \to 2\ell 2\mathrm{q}$, the WZ, ZZ, and DY events present in the SR are typically there because of misidentification of light-flavor, c quark, and gluon jets as b jets, since their matrix element does not have b quarks in its final state. In general, for each one of these processes, more than 80% of the events in the SR are there due to the misidentification of other jets as b jets. Naturally, this fraction is larger for the loose b tagging working point compared to stricter b tagging requirements.

5.3 Multivariate optimization

Fully connected multi-layer artificial neural networks, also known as multi-layer perceptrons (MLPs), are used to combine variables based on $\vec{p}_{\mathrm{T}}^{\,\mathrm{miss}}$ and information from the leptons into a single discriminant to sort the events in the SR into intervals of low to high sensitivity. The MLPs are implemented using the PyTorch package [87] and are trained on simulated events in the SR for each data-taking period.

The following variables are passed to the MLPs as input: $p_{\mathrm{T}}^{\ell_1}$, $p_{\mathrm{T}}^{\ell_2}$, $p_{\mathrm{T}}^{\ell\ell}$, $\Delta R^{\ell\ell}$, $\Delta m^{\ell\ell}$, $p_{\mathrm{T}}^{\mathrm{miss}}$, $m_{\mathrm{T}}^{\ell\ell,p_{\mathrm{T}}^{\mathrm{miss}}}$, $\Delta\phi^{\ell\ell,p_{\mathrm{T}}^{\mathrm{miss}}}$, and $m_{\mathrm{T2}}^{\ell\ell}$. The latter variable is useful to discriminate events from the decay of a primary particle into an invisible and a visible particle [85, 88]. It is related to the mass difference between the primary and the invisible particles,

$$m_{\mathrm{T2}}^{\ell\ell} = \min_{\vec{p}_{\mathrm{T},\bar{\nu}}+\vec{p}_{\mathrm{T},\nu}=\vec{p}_{\mathrm{T}}^{\,\mathrm{miss}}} \left[\max\{m_{\mathrm{T}}(m_\ell, m_{\bar{\nu}}, \vec{p}_{\mathrm{T},\ell}, \vec{p}_{\mathrm{T},\bar{\nu}}), m_{\mathrm{T}}(m_{\bar{\ell}}, m_\nu, \vec{p}_{\mathrm{T},\bar{\ell}}, \vec{p}_{\mathrm{T},\nu})\}\right], \tag{5.1}$$

with

$$m_{\mathrm{T}}(m_1, m_2, \vec{p}_{\mathrm{T},1}, \vec{p}_{\mathrm{T},2}) = \sqrt{m_1^2 + m_2^2 + 2(E_{\mathrm{T},1}E_{\mathrm{T},2} - \vec{p}_{\mathrm{T},1}\cdot\vec{p}_{\mathrm{T},2})}, \tag{5.2}$$

where m_i, $\vec{p}_{\mathrm{T},i}$, and $E_{\mathrm{T},i}$ are the mass, transverse momentum vector, and transverse energy of particle i, respectively.

Variables directly related to jet kinematics were not used as input to the MLP discriminator to avoid propagating to the MLP score their shape mismodeling. The incorrect modeling was observed in the CRs when comparing the MC distributions of these variables with those

JHEP06(2026)014

from data. Jet mismodeling may occur due to the intrinsic complexity in reconstructing a jet and due to neutrinos coming from hadronic decays inside the jet. The inclusion of $p_{\mathrm{T}}^{\mathrm{miss}}$ information in the input variables was important since it has a large discrimination power between signal and background events. However, since the $p_{\mathrm{T}}^{\mathrm{miss}}$ scale and resolution in DY simulation are more affected by jet mismodeling than in other processes, they needed to be corrected to match those in the data, as described in section 6.

During the training, the contributions from all processes are normalized to the integrated luminosity of the data and expected cross sections. The signal class groups events from all signal samples, while the background class groups events from all background processes. For each class, the sum of weights is then normalized to the same value to achieve equal statistical importance for both classes during the MLP training.

The MLP architectures with the best discrimination performance for each data-taking period are composed of two or three hidden layers and 20 nodes in each hidden layer. The input variables that contribute most to the discrimination performance are found to be $p_{\mathrm{T}}^{\mathrm{miss}}$ and $m_{\mathrm{T}}^{\ell\ell,p_{\mathrm{T}}^{\mathrm{miss}}}$, followed by $m_{\mathrm{T2}}^{\ell\ell}$ and $\Delta R^{\ell\ell}$, estimated using information from the permutation importance method [89]. Figure 2 shows a comparison between signal and background distributions in these variables in the SR, normalized to unit area. Since the WZ contribution comes from events with one lepton not reconstructed, its kinematic distributions are similar to the ones from ZZ. For this reason, these two backgrounds are combined in figure 2.

To construct the search intervals used to extract the signal, the MLP score is transformed into the MLP4 score, defined as

$$\text{MLP4 score} = \frac{10^{4\times\text{MLP score}}}{10^4}. \tag{5.3}$$

The MLP4 score, primarily based on statistical considerations, expands the region with a high sensitivity making the intervals in MLP4 more practical and effective.

In addition, we observe that the MLP4 score returns values close to 1 for more boosted signal samples (higher $p_{\mathrm{T}}^{\ell\ell}$), while less boosted signal samples (lower $p_{\mathrm{T}}^{\ell\ell}$) show a peak at slightly smaller values in the MLP4 score distribution. To maximize the sensitivity for both types of signal events, while preserving the smoothness of the distributions, we define the search intervals in the MLP4 score as

$$[0.00, 0.01, 0.08, 0.15, 0.22, 0.29, 0.36, 0.43, 0.50, 0.57, 0.64, 0.71, 0.78, 0.85, 0.90, 0.95, 0.98, 1.00],$$

in which smaller intervals are defined in the region closest to 1 in order to be sensitive to the shape variation of the different signal samples. Below 0.85, equal-size intervals are defined, except for the first interval, which is equal to 0.01 to avoid a large concentration of events there, most of them being background. The MLP4 bins will be labeled with integer numbers ranging from 1 to 17, indicating the position of the corresponding interval in the above definition.

6 Background estimation

The analysis relies partially on simulation to estimate the background contribution from SM processes. The $\mathrm{t\bar{t}}$ and WZ simulations are improved by applying NNLO(+NLO) corrections,

JHEP06(2026)014

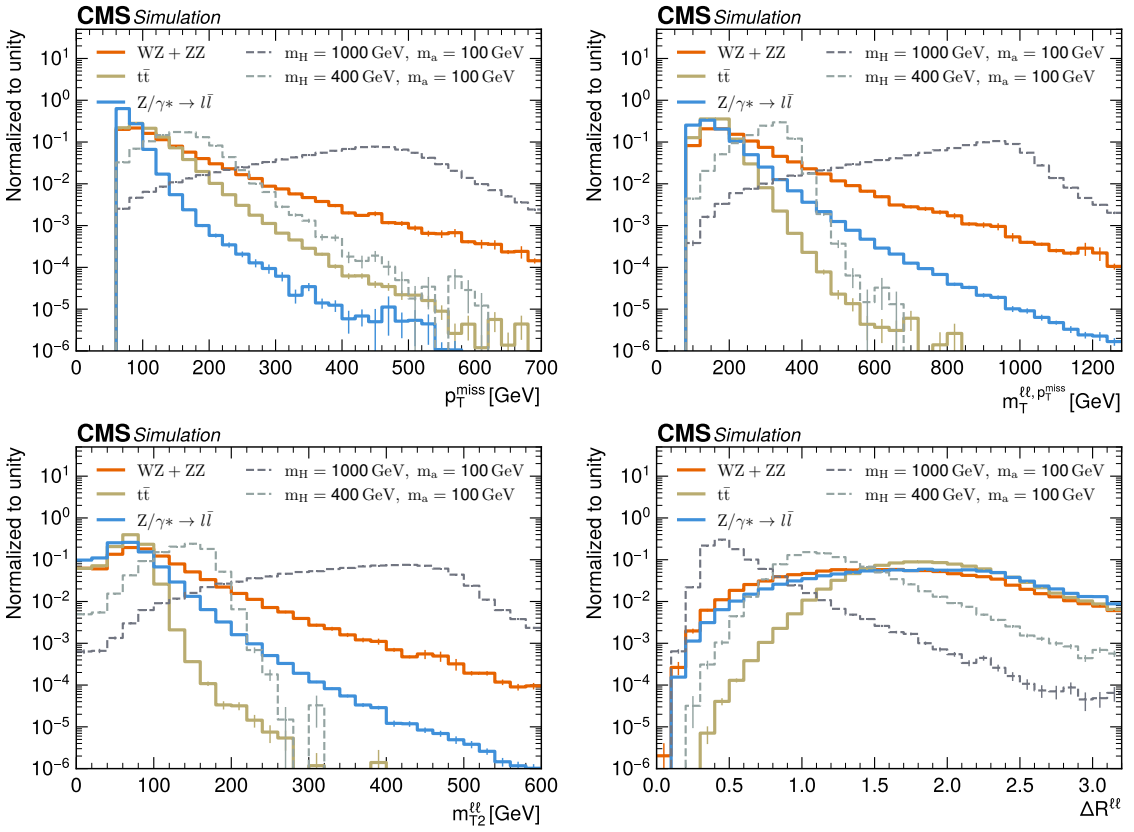

Figure 2. Normalized distributions in $p_{\mathrm{T}}^{\mathrm{miss}}$ (upper left), $m_{\mathrm{T}}^{\ell\ell,p_{\mathrm{T}}^{\mathrm{miss}}}$ (upper right), $m_{\mathrm{T2}}^{\ell\ell}$ (lower left), and $\Delta R^{\ell\ell}$ (lower right) in the SR for the main background processes (solid lines) and two signal samples representing extreme kinematic behaviors, which are obtained by considering high (dark gray dashed line) and low (light gray dashed line) values of m_{H} and $m_{\mathrm{H}} - m_{\mathrm{a}}$. The vertical bars at the center of the bins represent the statistical uncertainty in the predictions.

as described in section 3. In turn, the $p_{\mathrm{T}}^{\mathrm{miss}}$ scale and resolution in the DY simulation are corrected using an auxiliary measurement derived in a sideband region with $p_{\mathrm{T}}^{\mathrm{miss}} < 65\,\mathrm{GeV}$ and extrapolated to the main analysis region with larger values of $p_{\mathrm{T}}^{\mathrm{miss}}$. The measurement consists of propagating to $p_{\mathrm{T}}^{\mathrm{miss}}$ the correction of the parallel and orthogonal hadronic recoil projections on the direction of the reconstructed dilepton transverse momentum vector ($\vec{p_{\mathrm{T}}}^{\ell\ell}$). The correction is derived for different jet multiplicities and $p_{\mathrm{T}}^{\ell\ell}$ intervals using a parameterized double Gaussian function to match the simulation distributions to the ones in data. The extrapolation is verified in a region with no b jets and $p_{\mathrm{T}}^{\mathrm{miss}} < 300\,\mathrm{GeV}$, also dominated by DY events.

The normalization of the largest backgrounds in this search, namely DY, $\mathrm{t\bar{t}}$, WZ, and ZZ production, is corrected using a data-driven method. It makes use of unconstrained parameters associated with the normalization of each background process that are linked across various regions in a maximum likelihood fit to data (discussed in section 8). The definitions of the CRs are described below. Their corresponding purities are 95% (DY CR), 92% ($\mathrm{t\bar{t}}$ CR), 62% (WZ CR), and 95% (ZZ CR). We show a summary of the SR and CRs in figure 3, which illustrates the variables used to define the different regions.

JHEP06(2026)014

All CRs, except for the DY CR, must have $N_{\mathrm{b}} \geq 1$, identical to the SR, where N_{b} denotes the number of b jets. These regions contain a significant fraction of $\mathrm{t\bar{t}}$ events. To reduce the contributions from $\mathrm{t\bar{t}}$ production in the WZ and ZZ CRs, we discard events that have an analytic solution for the dileptonic $\mathrm{t\bar{t}}$ event reconstruction described in section 5.2. Additional requirements defining the CRs are listed below.

- As in the SR, events in the DY CR must have exactly two OSSF leptons. Events with $p_{\mathrm{T}}^{\mathrm{miss}} > 140\,\mathrm{GeV}$ are discarded to suppress a potential contamination from signal and other background processes. Events in the DY CR must have $N_{\mathrm{b}} = 0$. We checked the consistency between the normalization of DY events with $N_{\mathrm{b}} = 0$ and $N_{\mathrm{b}} \geq 1$ by comparing the ratio of the number of data and simulation events in additional regions with lower values of $p_{\mathrm{T}}^{\mathrm{miss}}$ ($< 40\,\mathrm{GeV}$ and between 40–65 GeV). We observe ratios that are compatible between the $N_{\mathrm{b}} = 0$ and $N_{\mathrm{b}} \geq 1$ categories, validating the use of the DY CR for correcting the DY normalization in the SR.

- In the $\mathrm{t\bar{t}}$ CR, events must have exactly two opposite-sign different-flavor (OSDF) leptons, i.e. $\mathrm{e^{+}\mu^{-}}$ or $\mathrm{e^{-}\mu^{+}}$, resulting in a region enriched with $\mathrm{t\bar{t}}$ events in the dilepton channel.

- In the WZ CR, events must have exactly two OSSF leptons and one additional lepton ℓ_3. To improve the purity of this CR in WZ events, we add the following requirements in well-reconstructed variables, $\Delta m^{\ell\ell} < 10\,\mathrm{GeV}$ and $m_{\mathrm{T}}^{\ell_3,p_{\mathrm{T}}^{\mathrm{miss}}} > 50\,\mathrm{GeV}$, where $m_{\mathrm{T}}^{\ell_3,p_{\mathrm{T}}^{\mathrm{miss}}}$ is the transverse mass of the ℓ_3 and $\vec{p}_{\mathrm{T}}^{\,\mathrm{miss}}$ system.

- In the ZZ CR, besides the two OSSF leptons with invariant mass closer to m_{Z}, two additional OSSF leptons, ℓ_3 and ℓ_4, are required. In addition, a condition on the reconstructed invariant mass of this extra dilepton system is imposed to remove contamination from other processes with negligible impact on the amount of ZZ events, namely $m^{\ell_3\ell_4} > 10\,\mathrm{GeV}$.

Intrinsically, the DY process does not have undetectable particles with large p_{T} in the final state, such that events with large $p_{\mathrm{T}}^{\mathrm{miss}}$ are rare. Nonnegligible values of $p_{\mathrm{T}}^{\mathrm{miss}}$ can originate from detector acceptance effects, as well as mismeasurements. For this reason, DY events contribute mostly to the region of small $p_{\mathrm{T}}^{\mathrm{miss}}$ and constitute an important background for signal samples with small $p_{\mathrm{T}}^{\ell\ell}$. On the other hand, ZZ and WZ production with large $p_{\mathrm{T}}^{\mathrm{miss}}$ are important backgrounds for signal samples with large $p_{\mathrm{T}}^{\ell\ell}$. In the SR, 91% of the ZZ events are those in which the second Z boson does not decay to charged leptons, while 66% of the WZ events have a W boson decaying to one neutrino and one charged lepton, which falls outside of the detector acceptance. To ensure consistency between quantities defined in SR and CRs, making the distribution in $p_{\mathrm{T}}^{\mathrm{miss}}$ from WZ and ZZ events in the CRs analogous to those in the SR, the additional leptons present in the WZ CR (ℓ_3) and ZZ CR (ℓ_3 and ℓ_4) are removed from the calculation of $p_{\mathrm{T}}^{\mathrm{miss}}$. This also increases the statistical precision of these CRs, because $p_{\mathrm{T}}^{\mathrm{miss}}$ increases and more events pass the $p_{\mathrm{T}}^{\mathrm{miss}} > 65\,\mathrm{GeV}$ requirement.

A comparison is made in each CR between data and simulation in the distributions of all MLP input variables to verify that the modeling is adequate for the different background

JHEP06(2026)014

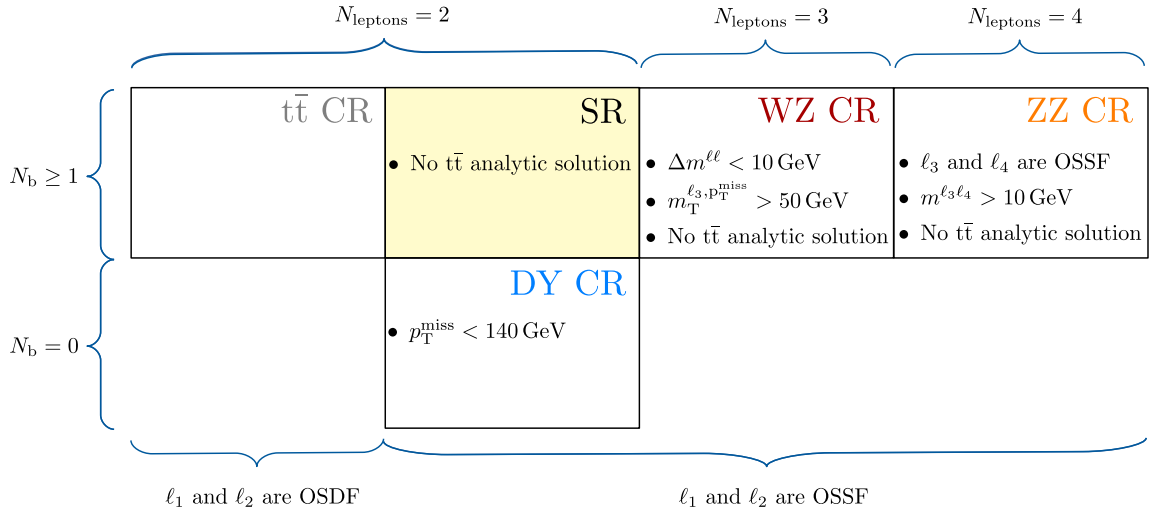

Figure 3. Illustration of the requirements on the SR and CRs. The regions are represented as blocks, and the requirements are denoted by curly brackets placed around the blocks and bullets within each block. All requirements are applied on top of the baseline selection.

processes. Because of its importance, the distributions in $p_{\text{T}}^{\text{miss}}$ after a background-only fit to the data in the four CRs is shown in figure 4. A maximum likelihood fit is performed on the $p_{\text{T}}^{\text{miss}}$ distribution, combining only the four CRs. The same group of systematic uncertainties described in section 7 is included in this fit. We observe agreement in shape and normalization between data and simulation within the uncertainties.

The distributions in the MLP4 score are compared between data and simulated events in the CRs to verify the modeling of the search variable. For this check, the granularity of the MLP4 score as defined for the SR is too high, because of the smaller statistical precision in the CRs, especially for the WZ and ZZ CRs. We merge several of the defined MLP4 bins in order to obtain a reasonable number of observed events in each bin of the MLP4 distributions in the CRs. The resulting distributions are shown in figure 5 after a background-only fit to the data in the CRs, which was executed in a similar way as done for $p_{\text{T}}^{\text{miss}}$. We observe a good modeling of the MLP4 score by the simulated SM processes that constitute the largest backgrounds in this search.

7 Systematic uncertainties

Several uncertainty sources of both experimental and theoretical nature are taken into consideration when performing the combined maximum likelihood fit described in section 8. These uncertainties can affect some or all simulated processes depending on their source. Most uncertainties in this analysis affect both the shape and normalization of the signal and background processes, except the uncertainty on the integrated luminosity, which only affects the overall rate. Various degrees of correlation for nuisance parameters arising from analogous subsidiary measurements performed in different data-taking conditions are considered.

Among the theoretical uncertainties affecting the shape and the normalization of all relevant processes are the renormalization and factorization scales in the ME calculation.

JHEP06(2026)014

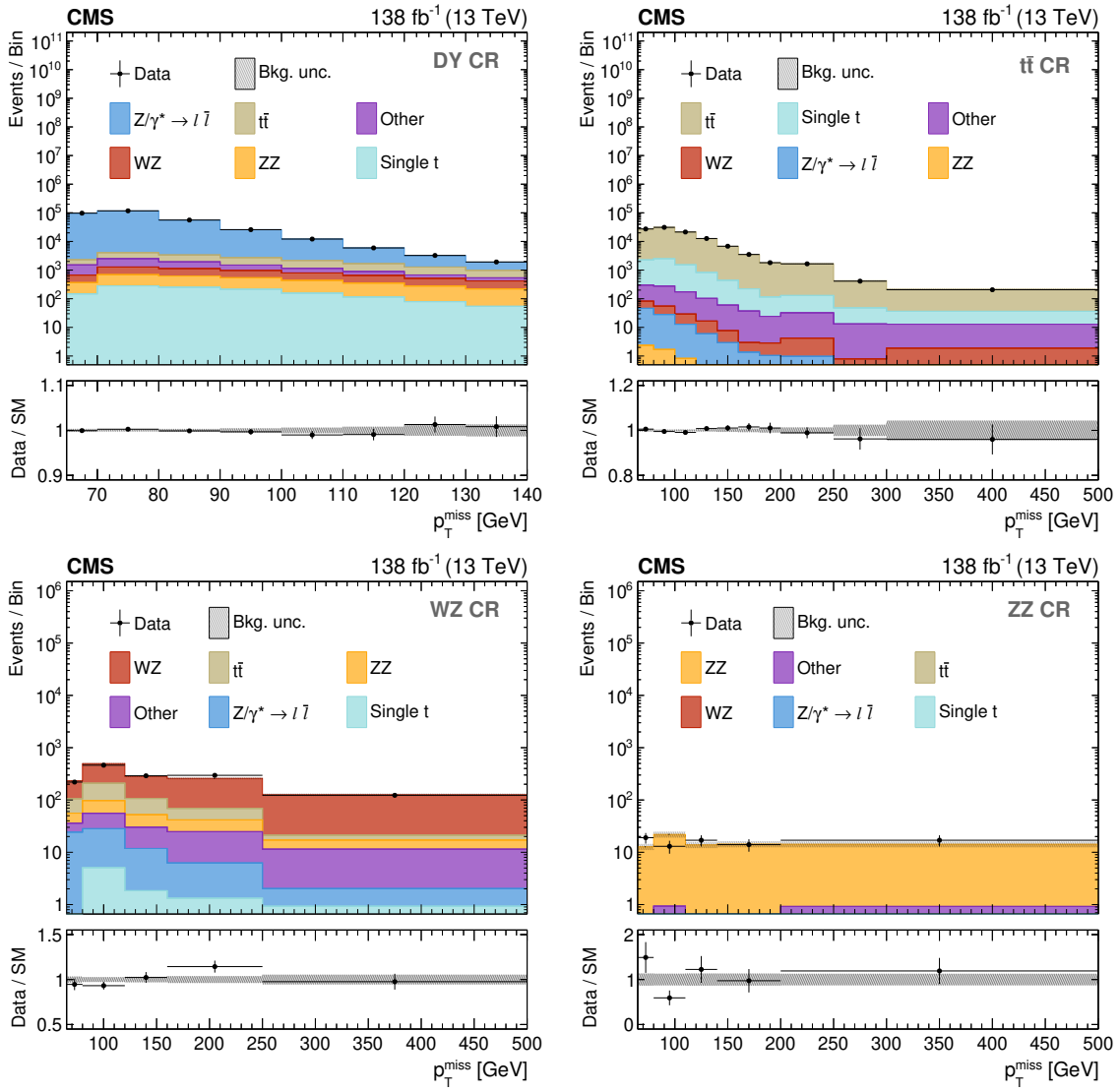

Figure 4. Distributions in $p_{\mathrm{T}}^{\mathrm{miss}}$ for the DY (upper left), $\mathrm{t\bar{t}}$ (upper right), WZ (lower left), and ZZ (lower right) CRs. In the WZ and ZZ CRs, $p_{\mathrm{T}}^{\mathrm{miss}}$ is obtained by removing the additional leptons from the calculation. The distributions are shown after performing a background-only fit in the $p_{\mathrm{T}}^{\mathrm{miss}}$ distributions of all CRs. The last bin includes the overflow, except for the DY CR where $p_{\mathrm{T}}^{\mathrm{miss}} < 140\,\mathrm{GeV}$. The lower panels show the post-fit values and uncertainties of the ratio between the observed data and the predicted SM backgrounds. The various background processes are represented by filled histograms. The data are shown as black circles, where the vertical bars represent the statistical uncertainty and the horizontal bars indicate the bin width.

JHEP06(2026)014

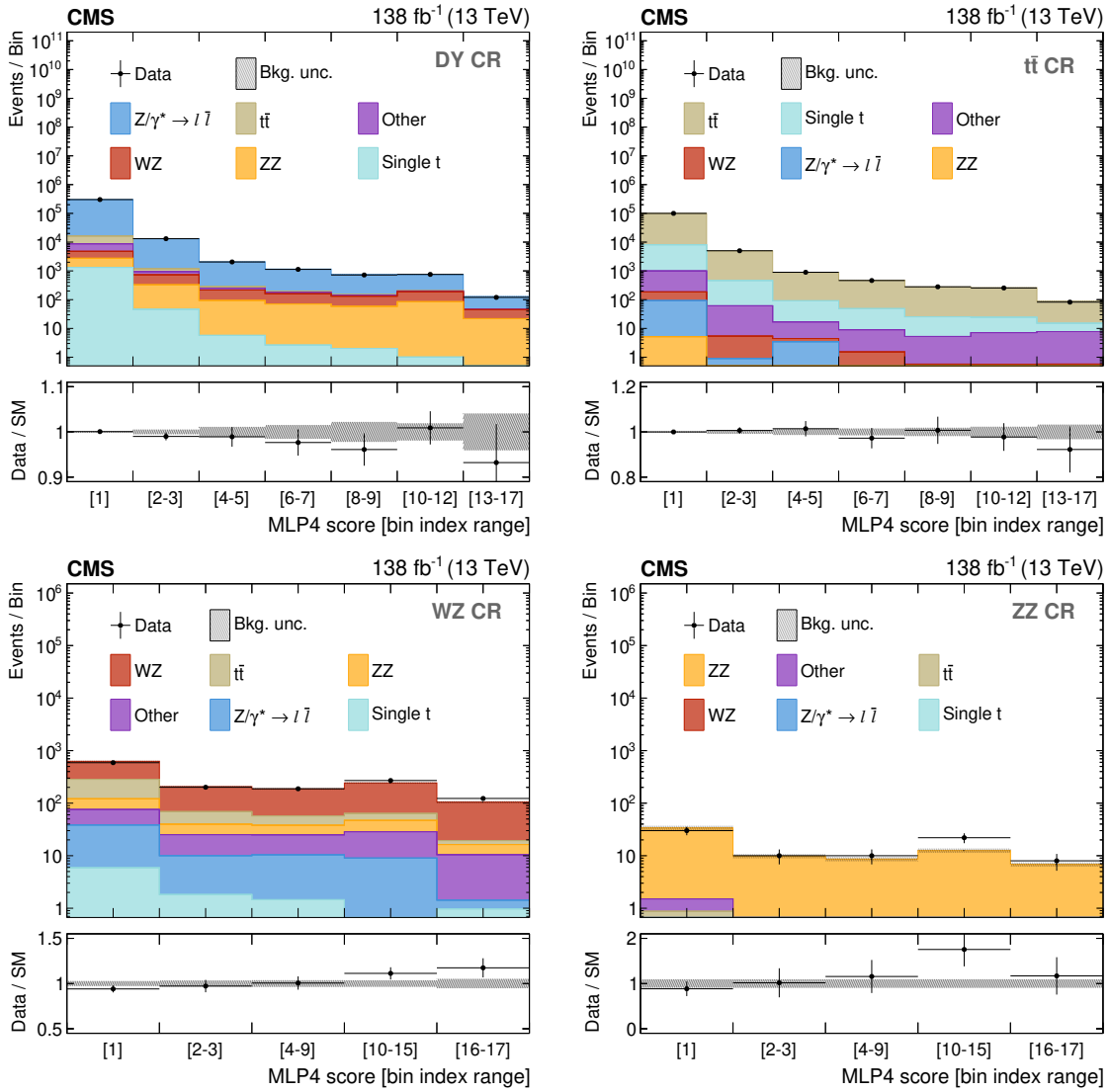

Figure 5. Distributions in the MLP4 score for the DY (upper left), $t\bar{t}$ (upper right), WZ (lower left), and ZZ (lower right) CRs. The distributions are shown after performing a background-only fit in the MLP4 score distributions of all CRs. The labels on the horizontal axes indicate the MLP4 intervals that define a given bin. The lower panels show the post-fit values and uncertainties of the ratio between the observed data and the predicted SM backgrounds. The various background processes are represented by filled histograms. The data are shown as black dots, where the vertical bars represent the statistical uncertainty and the horizontal bars indicate the bin width.

JHEP06(2026)014

Variations in these scales by a typical factor of two, in either one of them or both of them simultaneously, estimate the uncertainty from missing higher-order corrections, that can lead to changes of the differential cross sections as a function of various kinematic variables. This kinematic shape effect is then transferred to the MLP4 score and is thus considered in the analysis as a general shape effect for different signal and background processes. A similar procedure is used to estimate the uncertainty in the parton shower for the simulation of initial- and final-state radiation, where the scale of the strong coupling is changed by factors of 2 and 0.5. We use per-event weights [90, 91] to estimate the uncertainty in the PDFs used to generate the signal and background processes.

An uncertainty that is specific to the $\mathrm{t\bar{t}}$ background is related to the NNLO QCD (+ NLO EW) correction of the top quark p_{T} distribution applied to the NLO QCD generated sample, as described in section 3. The uncertainty in this correction is estimated by taking the difference between the case where this correction is applied and the one where it is not applied. This uncertainty is one of the largest uncertainties in the simulation of the $\mathrm{t\bar{t}}$ background. Analogously, for the correction applied to the WZ process that employs a similar level of accuracy as for the $\mathrm{t\bar{t}}$ process (see section 3), a comparable procedure is used. Because the WZ process contributes more significantly in the bins with the highest signal concentration, the associated uncertainty has a larger impact on the overall sensitivity than the analogous uncertainty in the $\mathrm{t\bar{t}}$ background, and it also dominates over the uncertainties from the DY-related $p_{\mathrm{T}}^{\mathrm{miss}}$ scale and resolution corrections.

Theoretical uncertainties can substantially reduce the analysis sensitivity in the model-specific interpretation, where the limited accuracy of the LO signal simulation introduces a normalization uncertainty of up to 20%. However, the experimental systematic uncertainties and the statistical uncertainties are the largest ones in this analysis. The statistical size of the CRs directly affects the normalization uncertainties in the corresponding SM processes. These uncertainties can have a large impact, especially on processes classified by the MLP4 score as more signal-like, such as ZZ and WZ. The proportion of these normalization uncertainties in the main backgrounds, primarily arising from the CR sample sizes, represents the leading factor determining the sensitivity of this search. Also, the limited size of some of the simulated event samples plays an important role in bins with very high values of the MLP4 score, where the background count is low. The statistical uncertainties from the limited size of simulated samples are modeled with the Barlow-Beeston method [92].

An important group of experimental uncertainty sources is related to the identification, reconstruction, and triggering efficiencies of the lepton candidates [75, 76, 93]. These uncertainties also include uncertainties in data-to-simulation correction factors that affect the shape of the various processes. The uncertainties in the reconstruction and identification of individual electron candidates range between 1.0 and 2.5%, and for muons these amount to about 1.0% in the identification and 0.5% in the isolation requirements. The total uncertainty associated with the trigger efficiency is approximately 3%. Due to an early timing offset in the muon and ECAL trigger signals (so-called L1 trigger prefiring) during certain data-taking periods, a correction in simulation and its corresponding systematic uncertainty were included. Depending on the selection region and the kinematic properties of the specific

JHEP06(2026)014

process, this translates into an uncertainty of a few percent in the normalization of the signal and background processes.

Uncertainties in the reconstruction of jets as well as in $p_{\mathrm{T}}^{\mathrm{miss}}$ are also relevant, most notably the jet energy scale and resolution, and the unclustered energy component of $p_{\mathrm{T}}^{\mathrm{miss}}$. The change in normalization from the latter uncertainty can be as large as 10% for some processes such as DY. This process is particularly sensitive to systematic effects in the misreconstruction of $p_{\mathrm{T}}^{\mathrm{miss}}$, where nonnegligible values arise from the limited precision in the reconstruction of jets and unclustered particles.

The b-tagging efficiency is corrected in simulation to match the one observed in data through an event-by-event reweighting [82]. The effect of the corresponding uncertainty on the signal normalization is around 2–3% on average, while for processes with a larger number of b-tagged jets, such as $\mathrm{t\bar{t}}$ production, it can be as large as 6%. As expected, the uncertainty related to the b-tagging efficiency in the analysis has primarily an impact on the normalization of the simulated processes.

The uncertainty associated with the scale and resolution correction applied to $p_{\mathrm{T}}^{\mathrm{miss}}$ of the DY process has a direct impact on the most important input variables to the MLP classifier, such as $p_{\mathrm{T}}^{\mathrm{miss}}$ itself and $m_{\mathrm{T}}^{\ell\ell,p_{\mathrm{T}}^{\mathrm{miss}}}$. This is an important experimental uncertainty for signal hypotheses with small $p_{\mathrm{T}}^{\ell\ell}$ that tend to have a slightly lower MLP4 score.

The simulated samples are reweighted to reproduce the distribution in the number of pileup interactions observed in data. A corresponding uncertainty is estimated by recalculating these weights for variations in the total inelastic cross section by ±5% [94].

The last experimental systematic source is the integrated luminosity for each data-taking period (2016, 2017, and 2018), accounting for an associated uncertainty of 1.2–2.5% [95–97], with an overall uncertainty for 2016–2018 data amounting to 1.6%. This uncertainty affects the rate of the simulated signal and minor background processes estimated entirely from the simulation.

The maximum magnitude of the various systematic uncertainties affecting the signal and background processes, averaged across the individual analysis categories and processes, is shown in table 2.

8 Results

A combined maximum likelihood fit [98] across all regions is performed using a binned discriminator obtained from the MLP4 score in the SR and single bins in the CRs. The probability density functions of both hypotheses under consideration (background-only and signal-plus-background) are obtained primarily by means of MC simulation, with appropriate corrections determined from subsidiary measurements in the data. These functions are constructed by employing histogram templates. For the SR, the templates are divided into 17 bins according to the MLP4 score output, as indicated in section 5.3.

In each of the CRs, a single-bin subsidiary measurement is performed, which creates a link between processes across all the regions. This way, the normalizations of the dominant background processes as obtained from the corresponding CRs are corrected in all regions simultaneously, especially in the SR. The single-bin subsidiary measurements constrain the parameters connected to the systematic uncertainties and correct any bias in the normalization

JHEP06(2026)014

Systematics	Type	Size
Integrated luminosity	lnN	<2.5%
Pileup reweighting	shape+ lnN	3.5%
b tagging efficiency	shape+ lnN	<5.9%
Electron reconstruction and identification	shape+ lnN	3.2%
Muon identification and isolation	shape+ lnN	3.0%
Trigger	shape+ lnN	2.9%
L1 prefiring	shape+ lnN	1.3%
Jet energy scale	shape+ lnN	3.1%
Jet energy resolution	shape+ lnN	2.5%
Jet pileup identification	shape+ lnN	2.1%
Unclustered energy $p_{\mathrm{T}}^{\mathrm{miss}}$	shape+ lnN	3.3%
Scale and resolution $p_{\mathrm{T}}^{\mathrm{miss}}$ DY	shape+ lnN	4.5%
W boson p_{T} correction WZ	shape+ lnN	4.4%
Top quark p_{T} correction $\mathrm{t\bar{t}}$	shape+ lnN	1.9%
Renormalization and factorization scales	shape+ lnN	<20%
PDF	shape+ lnN	<2.9%
Parton shower	shape+ lnN	<5.7%

Table 2. Displayed are the maximum variations arising from systematic uncertainties that influence the shape and normalization (lnN) of the signal and background processes. Only sources with an impact larger than 1% are reported.

of the process arising due to limited knowledge and modeling. In this way, effects related to either the limited accuracy in the cross sections of the background processes, or small calibration differences between MC samples and the data can be addressed.

The above description is depicted in figure 6, where the different contributions are shown after performing a background-only fit to the data. The left panel (first four bins) shows the CRs of the analysis, while the remaining bins show the search intervals for the MLP4 discriminator in the SR, with the y axis indicating the total number of events selected. During the fit the normalization of each relevant background process is adjusted to match the data in these CRs. With this procedure, the normalizations of the largest background processes are changed, increasing by 10 and 8% for DY and $\mathrm{t\bar{t}}$, respectively. The relative uncertainties on the estimated normalizations for DY and $\mathrm{t\bar{t}}$ are 0.5% and 0.8%, respectively. The changes in normalization obtained for WZ and ZZ are much larger, resulting in an increase of 101 and 113%, respectively, of the total yields. The relative uncertainties on the estimated normalizations for WZ and ZZ are 6% and 10%, respectively. The larger normalization factors for WZ and ZZ are understood and associated with the specific phase space probed, in particular, the simultaneous requirements of a large $p_{\mathrm{T}}^{\mathrm{miss}}$ and the presence of b jets. Previous CMS analyses, such as ref. [29], have already observed discrepancies in the modeling of WZ

JHEP06(2026)014

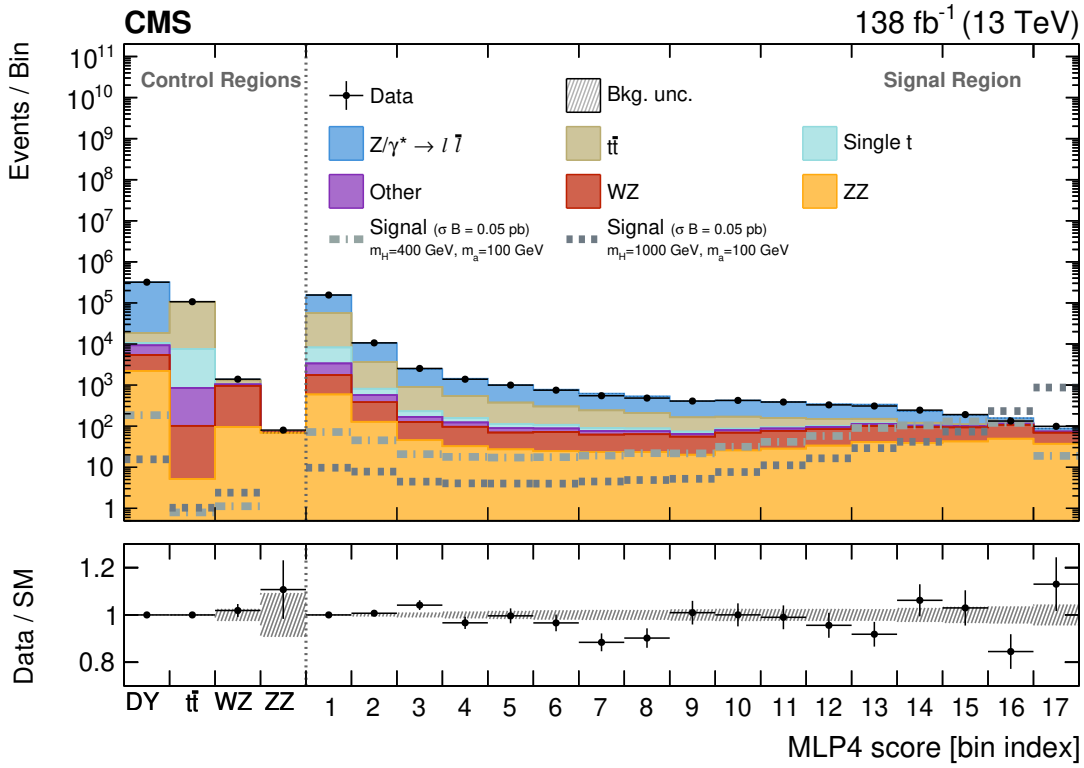

Figure 6. Main statistical discriminant of the analysis used to extract the signal after having performed a background-only fit to the observed data. The left side of the upper panel, separated by a vertical dotted line from the right side, shows the four CRs used to estimate the normalization of the main background processes entering the SR. The right side shows the full MLP4 score distribution in the SR used to discriminate between signal and background. The various background processes are represented by filled histograms. The data points are shown as black dots, with vertical bars representing the statistical uncertainty and horizontal bars indicating the bin width, while the signal scenarios under consideration are represented with a dashed-dotted line. The benchmark signal cross section is set to 0.05 pb for proper visualization purposes. The figure comprises the full combination of all final states and categories for the full data set. The lower panel shows the post-fit values and uncertainties of the ratio between the observed data and the predicted SM background.

and ZZ processes in phase-space regions with similar $p_{\mathrm{T}}^{\mathrm{miss}}$ requirements. Given that this search further requires a minimum number of b jets, and in view of the well-known limitations in the description of diboson production with additional b quarks, it is well motivated to expect an additional, non-negligible contribution to the overall mismodeling from this source. Note additionally that, in this work, the diboson cross sections are taken primarily at NLO accuracy, since the fit can naturally absorb residual corrections to the overall normalization of background processes independently of the initial pre-fit values. Several higher-order QCD calculations [99–101] have nevertheless demonstrated that corrections beyond this order can be sizable for the WZ and ZZ processes.

The results of the background-only fit reveal a good level of agreement between the SM prediction and the observed data. The maximum local significance for an excess of events over the SM prediction is below 0.7 standard deviation and occurs for the signal hypothesis

JHEP06(2026)014

with $m_{\mathrm{H}} = 2000\,\mathrm{GeV}$ and $m_{\mathrm{a}} = 400\,\mathrm{GeV}$. Although the dominant backgrounds are DY and $\mathrm{t\bar{t}}$ production in the dilepton final state, the WZ and ZZ processes tend to be classified as being more signal-like. For these two background processes, events featuring a reconstructed Z boson accompanied by substantial $p_{\mathrm{T}}^{\mathrm{miss}}$ are more prevalent, for the reasons discussed in section 3. This leads to the uncertainties in the normalization of these EW processes playing an essential role, becoming the most important systematic uncertainties in this analysis. As seen in the signal distributions, the MLP4 score tends to have higher values for signal events. This is illustrated for two signal mass configurations with $m_{\mathrm{H}} = 400$ and $1000\,\mathrm{GeV}$ for $m_{\mathrm{a}} = 100\,\mathrm{GeV}$. Depending on the mass difference $m_{\mathrm{H}} - m_{\mathrm{a}}$, the concentration of signal events at high values of the MLP4 discriminator will be higher or lower for large and small values of the mass difference, respectively.

8.1 Upper limits on the signal cross sections

The results from the maximum likelihood fits are used to set upper limits at 95% confidence level (CL) on the product of the cross section and branching fraction $\sigma\mathcal{B} = \sigma(\mathrm{pp} \to \mathrm{b\bar{b}H})\,\mathcal{B}(\mathrm{H} \to \mathrm{Za})\mathcal{B}(\mathrm{Z} \to l\bar{l})\mathcal{B}(\mathrm{a} \to \chi\bar{\chi})$. The exclusion limits are calculated using the asymptotic approximation of the $\mathrm{CL_s}$ method [102, 103].

Under the assumption that the narrow-width approximation is valid for all resonances involved in the decay chain, the computed upper limits only depend on the masses of the new resonances involved, i.e., m_{H} and m_{a}. Those limits can be translated into constraints on the parameters of a concrete model via the dependence of the cross section and branching fractions.

Figure 7 shows the observed and expected upper limits on the product of the cross section and branching fraction as function of the masses of the two resonances. The two-dimensional (2D) dependence has been unrolled into a one-dimensional graphic for better illustration, i.e. each limit band depicted along the y axis corresponds to a fixed value of m_{H}, while the dependency on m_{a} is given along the x axis. The expected and observed limits at 95% CL range from 10^{-3} to $10^{-2}\,\mathrm{pb}$. The discrepancies with a statistical deviation greater than one standard deviation, observed in the limits for the signal hypothesis with lower m_{H} and $m_{\mathrm{H}} - m_{\mathrm{a}}$, are associated with the small deficit seen around bin 16 in the MLP4 distribution in SR, since these signal hypotheses have their peak in bins just below bin 17.

The analysis is sensitive to semi-boosted scenarios, namely when the mass difference $m_{\mathrm{H}} - m_{\mathrm{a}}$ is around 1 TeV. For very small mass differences, the selection requirements imposed on leptons and $p_{\mathrm{T}}^{\mathrm{miss}}$ tend to have an important impact on the signal acceptance, as it usually happens in compressed scenarios [104, 105], where the energy of the decay products is not sufficient to pass the minimal p_{T} requirements on the physics objects. On the other hand, when the mass difference is too large, the leptonic products arising from the decay of the Z bosons start to overlap in the (η, ϕ) space, thus making the successful reconstruction and identification of the leptonic pair increasingly less likely.

8.2 Interpretation in the 2HDM+a context

The results on $\sigma\mathcal{B}$ are translated into constraints on the parameters of the 2HDM+a model using the benchmark scenario specified in eq. (3.1). We verified that the effect of the parameter variations is negligible in the kinematic distributions of the signal samples in the probed

JHEP06(2026)014

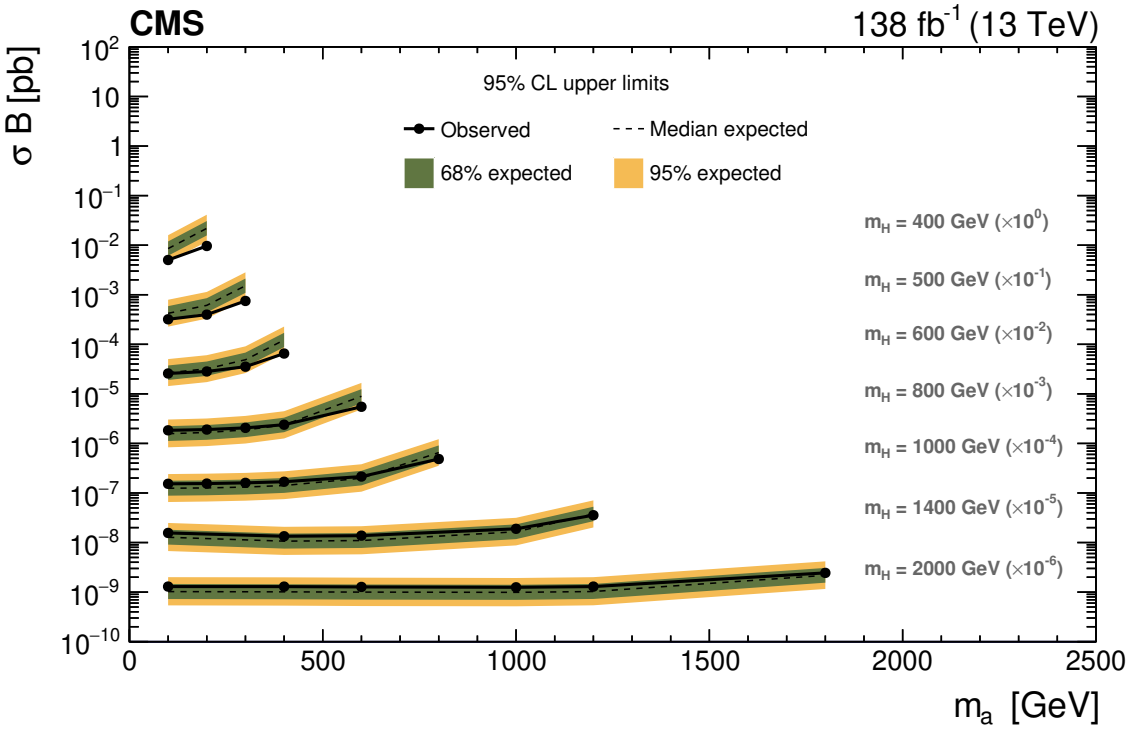

Figure 7. Observed and expected upper limits at 95% CL on the product of the signal cross section and branching fractions $\sigma\mathcal{B}$. The dependence of the limits on the pair $(m_{\mathrm{H}}, m_{\mathrm{a}})$ has been accommodated into various 1D projections for a fixed value of m_{H}, where the corresponding limits have been scaled by an arbitrary factor $(\times 10^{-n})$ for visualization purposes. The y axis contains the obtained cross section upper limit for the various combinations, whereas the x axis exhibits the dependence on the mass of the pseudoscalar. The solid and dashed lines correspond to the observed and median expected limits, respectively, while the green and yellow bands indicate the regions that contain 68% and 95% of the expected upper limits.

parameter space. A summary of the latest experimental constraints on the 2HDM+a model, obtained from searches targeting a variety of final states, can be found in refs. [5, 8].

Four relevant parameters are simultaneously varied to estimate the dependence of $\sigma\mathcal{B}$: m_{H}, m_{a}, $\tan\beta$, and $\sin\theta$. The calculations are performed using MG5 and the MadWidth [106] functionality within it. Several 2D projections of the constraints are constructed by varying two of the above parameters while keeping the rest fixed to their values in eq. (3.1). A 2D interpolation procedure is used to obtain the values for mass configurations that are not generated and parameter values for which the cross sections have not been calculated. In cases where one of the masses m_{H} or m_{a} is fixed, the values $m_{\mathrm{H}} = 800\,\mathrm{GeV}$ and $m_{\mathrm{a}} = 300\,\mathrm{GeV}$ are chosen. For each of these configurations in the 2HDM+a, we delimit regions favored by DM relic density calculations, obtained by assuming a velocity-averaged annihilation cross section to be in the range $\langle\sigma v\rangle = (2\text{–}4)\times 10^{-26}\,\mathrm{cm}^3/\mathrm{s}$. Those calculations were done using the MadDM tool [107]. The above interval is constructed by varying the canonical value obtained for the thermally averaged cross section at the time of freeze-out, resulting from the observed DM relic abundance [108]. This value corresponds to $\langle\sigma v\rangle \approx 3\times 10^{-26}\,\mathrm{cm}^3/\mathrm{s}$ [109].

JHEP06(2026)014

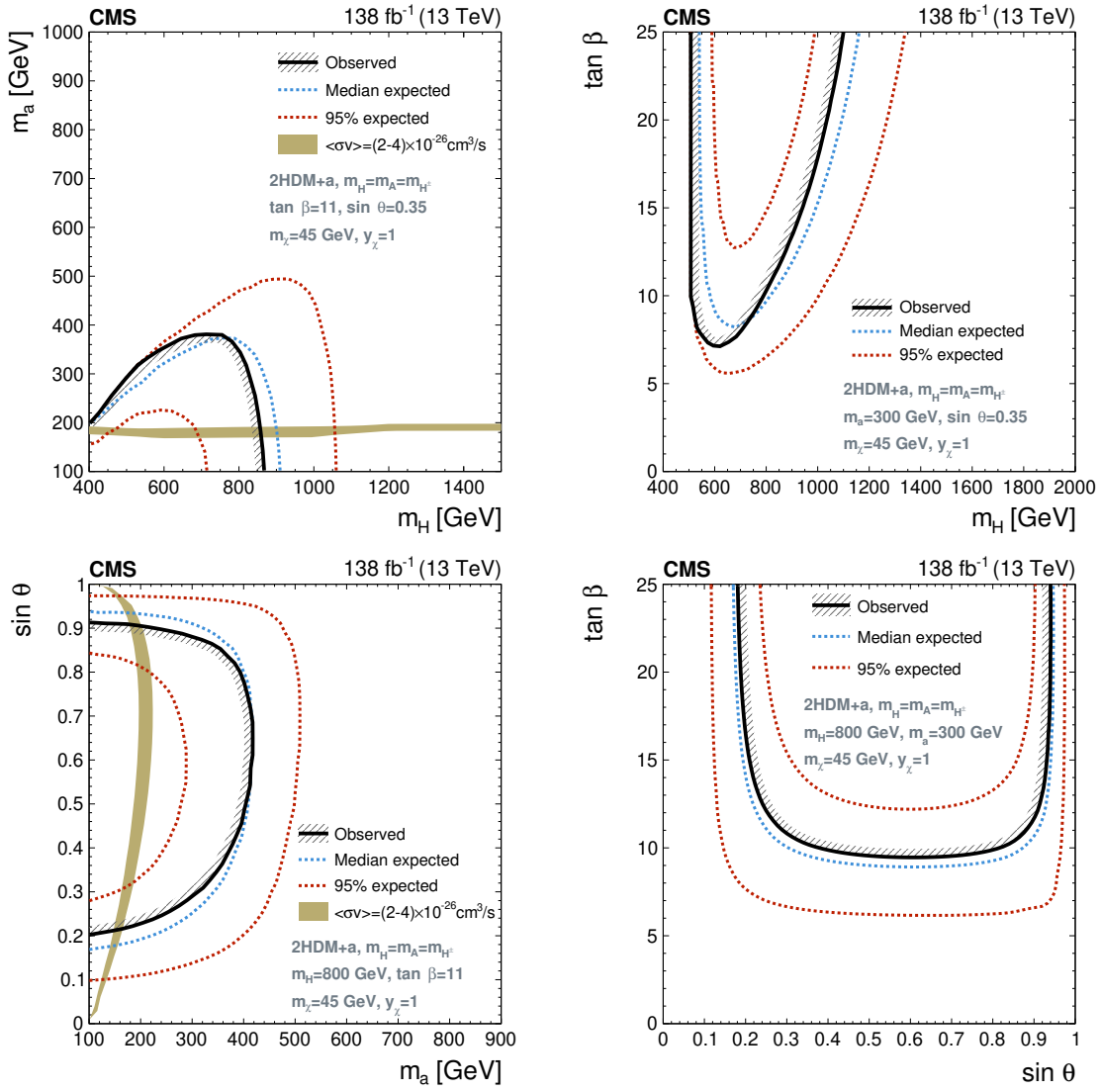

Figure 8. Excluded regions in the parameter space of the 2HDM+a. The solid lines encompass the observed excluded regions, the dashed blue lines the expected, and the red-dotted lines indicate the regions that contain 95% of the expected exclusion limits. Projections are presented for the (m_{H}, m_{a}) plane (upper left), (m_{H}, $\tan\beta$) plane (upper right), (m_{a}, $\sin\theta$) plane (lower left), and ($\tan\beta$, $\sin\theta$) plane (lower right), for fixed values of the parameters in eq. (3.1). The olive green band represents the allowed region as estimated from $\langle\sigma v\rangle = (2\text{–}4)\times10^{-26}\,\mathrm{cm}^3/\mathrm{s}$, which covers a range around the central value required by the observed DM relic. The cases where this curve is not visible in the figures correspond to the scenario where the preferable values of $\tan\beta$ for this range of $\langle\sigma v\rangle$ fall beyond the threshold ($\tan\beta > 25$) depicted in the projections.

We then choose to vary it by one third up and down to construct a conservative coverage interval around the central value, similarly as suggested in ref. [3].

In figure 8, four projections of the exclusion regions in the various 2D planes are shown. In the (m_{H}, m_{a}) projection (upper left plot), one can observe that the analysis is able to exclude masses of the heavy scalar of up to 900 GeV for small masses of the pseudoscalar

JHEP06(2026)014

mediator. This is consistent with what was observed in a previous CMS search [29]. The previous study was not optimized for the associated production of H boson with b quarks, and thus could not access scenarios with high values of $\tan\beta$. In the (m_{H}, $\tan\beta$) projection (upper right plot), it is visible that the analysis is mainly sensitive to regions of the parameter space of large values of $\tan\beta$. For the chosen parameter values in this article, the analysis is able to exclude masses of the heavy scalar close to 1.1 TeV for values of $\tan\beta \sim 25$. In this particular projection, one can observe that, given that m_{a} is fixed to 300 GeV, values of m_{H} below 500 GeV are almost inaccessible for this analysis. This is caused by both the dramatic reduction of phase space, thus impacting $\mathcal{B}(\mathrm{H} \to \mathrm{Za})$, and lower sensitivity to less boosted mass configurations. The same behavior regarding very compressed mass configurations can be seen in the (m_{a}, $\sin\theta$) projection (lower left plot), where one observes that the analysis is not capable of excluding masses of the pseudoscalar larger than 400 GeV, given that the heavy scalar mass has been fixed to 800 GeV. However, the analysis is able to cover a large part of the parameter space for $m_{\mathrm{a}} < 400$ GeV, because of a multiplicative factor proportional to $\sin^2\theta\cos^2\theta$ in the partial decay width of $\mathrm{H} \to \mathrm{Z}a$. This projection shows the capability of this analysis to exclude regions of the parameter space that are favored by the cosmological estimations of the DM relic density, assuming the 2HDM+a and considering the preference towards high values of $\tan\beta$ [3]. This analysis excludes the low-m_{a} regions for a very broad range of values of $\sin\theta$, leaving only corners with very small or very large values of $\sin\theta$ uncovered. The last projection (lower right plot) onto the ($\tan\beta$, $\sin\theta$) plane shows the sensitivity of this analysis to intermediate values of $\sin\theta$, where a large part of the parameter space is excluded for $\tan\beta > 9$ for fixed values of m_{a} and m_{H}. As $\sin\theta$ approaches 0 or 1, the resulting limits deteriorate significantly, reflecting the corresponding suppression of the $\mathrm{H} \to \mathrm{Za}$ and $\mathrm{a} \to \chi\overline{\chi}$ decay modes. A change in the values of m_{a} and m_{H}, most importantly in the mass difference, causes an increase or decrease of the excluded region for larger or smaller mass differences, respectively.

9 Summary

The first dedicated search for dark matter (DM) with the CMS experiment has been presented, where the DM particles are produced through the production of a heavy neutral Higgs boson (H) in association with a bottom quark-antiquark ($\mathrm{b\overline{b}}$) pair, followed by the decay $\mathrm{H} \to \mathrm{Za}$ with $\mathrm{a} \to \chi\overline{\chi}$, where a is a pseudoscalar mediator and $\chi\overline{\chi}$ denote the DM particle and antiparticle. A data set of proton-proton collisions at a center-of-mass energy of 13 TeV, corresponding to an integrated luminosity of 138 fb^{-1}, is analyzed.

This analysis exploits for the first time a signature involving a Z boson decaying into a pair of electrons or muons combined with requirements on the number of b jets and the amount of missing transverse momentum. A discriminator obtained with machine-learning techniques is used to separate the signal from background events. The multivariate classifier is trained to reach a high level of discrimination across a broad range of kinematic variations that arise from the different configurations in which the Z boson and the DM mediator are produced.

No signs of DM production via the channel investigated here have been observed. The results are presented in terms of limits on the product of signal cross section and branching fractions for the decays $\mathrm{H} \to \mathrm{Za}$, $\mathrm{a} \to \chi\overline{\chi}$, and $\mathrm{Z} \to l\bar{l}$, where l denotes a charged lepton.

JHEP06(2026)014

The 95% confidence level upper limits for the production cross section branching fraction of the new particles vary between 10^{-2} and 10^{-3} pb for heavy Higgs masses between 400 and 2000 GeV, respectively. Constraints on the parameter space of a two Higgs doublet model plus a pseudoscalar (2HDM+a) benchmark are derived. Exclusion regions in two-dimensional planes formed from four relevant 2HDM+a parameters are shown. The results are compared with expectations for this model in the context of cosmological predictions, in particular with the constraints arising from the thermally averaged cross section at the time of freeze-out, which are dictated by the observed DM relic abundance. The experimental results exclude a significant region of the parameter space preferred by those predictions for some relevant scenarios of the 2HDM+a model.

Acknowledgments

We congratulate our colleagues in the CERN accelerator departments for the excellent performance of the LHC and thank the technical and administrative staffs at CERN and at other CMS institutes for their contributions to the success of the CMS effort. In addition, we gratefully acknowledge the computing centers and personnel of the Worldwide LHC Computing Grid and other centers for delivering so effectively the computing infrastructure essential to our analyses. Finally, we acknowledge the enduring support for the construction and operation of the LHC, the CMS detector, and the supporting computing infrastructure provided by the following funding agencies: SC (Armenia), BMBWF and FWF (Austria); FNRS and FWO (Belgium); CNPq, CAPES, FAPERJ, FAPERGS, and FAPESP (Brazil); MES and BNSF (Bulgaria); CERN; CAS, MoST, and NSFC (China); MINCIENCIAS (Colombia); MSES and CSF (Croatia); RIF (Cyprus); SENESCYT (Ecuador); ERC PRG, TARISTU24-TK10 and MoER TK202 (Estonia); Academy of Finland, MEC, and HIP (Finland); CEA and CNRS/IN2P3 (France); SRNSF (Georgia); BMFTR, DFG, and HGF (Germany); GSRI (Greece); NKFIH (Hungary); DAE and DST (India); IPM (Iran); SFI (Ireland); INFN (Italy); MSIT and NRF (Republic of Korea); MES (Latvia); LMTLT (Lithuania); MOE and UM (Malaysia); BUAP, CINVESTAV, CONACYT, LNS, SEP, and UASLP-FAI (Mexico); MOS (Montenegro); MBIE (New Zealand); PAEC (Pakistan); MES, NSC, and NAWA (Poland); FCT (Portugal); MESTD (Serbia); MICIU/AEI and PCTI (Spain); MOSTR (Sri Lanka); Swiss Funding Agencies (Switzerland); MST (Taipei); MHESI (Thailand); TUBITAK and TENMAK (Türkiye); NASU (Ukraine); STFC (United Kingdom); DOE and NSF (U.S.A.).

Individuals have received support from the Marie-Curie program and the European Research Council and Horizon 2020 Grant, contract Nos. 675440, 724704, 752730, 758316, 765710, 824093, 101115353, 101002207, 101001205, and COST Action CA16108 (European Union); the Leventis Foundation; the Alfred P. Sloan Foundation; the Alexander von Humboldt Foundation; the Science Committee, project no. 22rl-037 (Armenia); the Fonds pour la Formation à la Recherche dans l'Industrie et dans l'Agriculture (FRIA) and Fonds voor Wetenschappelijk Onderzoek contract No. 1228724N (Belgium); the Beijing Municipal Science & Technology Commission, No. Z191100007219010, the Fundamental Research Funds for the Central Universities, the Ministry of Science and Technology of China under Grant No. 2023YFA1605804, the Natural Science Foundation of China under Grant No. 12061141002, 12535004, and USTC Research Funds of the Double First-Class Initiative No. YD2030002017

JHEP06(2026)014

(China); the Ministry of Education, Youth and Sports (MEYS) of the Czech Republic; the Shota Rustaveli National Science Foundation, grant FR-22-985 (Georgia); the Deutsche Forschungsgemeinschaft (DFG), among others, under Germany's Excellence Strategy — EXC 2121 "Quantum Universe" — 390833306, and under project number 400140256 — GRK2497; the Hellenic Foundation for Research and Innovation (HFRI), Project Number 2288 (Greece); the Hungarian Academy of Sciences, the New National Excellence Program — ÚNKP, the NKFIH research grants K 131991, K 133046, K 138136, K 143460, K 143477, K 146913, K 146914, K 147048, 2020-2.2.1-ED-2021-00181, TKP2021-NKTA-64, and 2021-4.1.2-NEMZ_KI-2024-00036 (Hungary); the Council of Science and Industrial Research, India; ICSC — National Research Center for High Performance Computing, Big Data and Quantum Computing, FAIR — Future Artificial Intelligence Research, and CUP I53D23001070006 (Mission 4 Component 1), funded by the NextGenerationEU program (Italy); the Latvian Council of Science; the Ministry of Education and Science, project no. 2022/WK/14, and the National Science Center, contracts Opus 2021/41/B/ST2/01369, 2021/43/B/ST2/01552, 2023/49/B/ST2/03273, and the NAWA contract BPN/PPO/2021/1/00011 (Poland); the Fundação para a Ciência e a Tecnologia, grant CEECIND/01334/2018 (Portugal); the National Priorities Research Program by Qatar National Research Fund; MICIU/AEI/10.13039/501100011033, ERDF/EU, "European Union NextGenerationEU/PRTR", and Programa Severo Ochoa del Principado de Asturias (Spain); the Chulalongkorn Academic into Its 2nd Century Project Advancement Project, the National Science, Research and Innovation Fund program IND_FF_68_369_2300_097, and the Program Management Unit for Human Resources & Institutional Development, Research and Innovation, grant B39G680009 (Thailand); the Kavli Foundation; the Nvidia Corporation; the SuperMicro Corporation; the Welch Foundation, contract C-1845; and the Weston Havens Foundation (U.S.A.).

Data Availability Statement. Release and preservation of data used by the CMS Collaboration as the basis for publications is guided by the CMS data preservation, re-use, and open access policy.

Code Availability Statement. The CMS core software is publicly available on GitHub.

References

[1] G. Steigman and M.S. Turner, *Cosmological constraints on the properties of weakly interacting massive particles*, *Nucl. Phys. B* **253** (1985) 375 [INSPIRE].

[2] L. Roszkowski, E.M. Sessolo and S. Trojanowski, *WIMP dark matter candidates and searches — current status and future prospects*, *Rept. Prog. Phys.* **81** (2018) 066201 [arXiv:1707.06277] [INSPIRE].

[3] P. Tunney, J.M. No and M. Fairbairn, *Probing the pseudoscalar portal to dark matter via $\bar{b}bZ(\to \ell\ell)+ \not{E}_T$: from the LHC to the galactic center excess*, *Phys. Rev. D* **96** (2017) 095020 [arXiv:1705.09670] [INSPIRE].

JHEP06(2026)014

[4] G. Bertone, D. Hooper and J. Silk, *Particle dark matter: evidence, candidates and constraints*, *Phys. Rept.* **405** (2005) 279 [hep-ph/0404175] [INSPIRE].

[5] CMS collaboration, *Dark sector searches with the CMS experiment*, *Phys. Rept.* **1115** (2025) 448 [arXiv:2405.13778] [INSPIRE].

[6] A. De Roeck, *Dark matter searches at accelerators*, *Nucl. Phys. B* **1003** (2024) 116480 [INSPIRE].

[7] ATLAS collaboration, *Constraints on simplified dark matter models involving an s-channel mediator with the ATLAS detector in pp collisions at* $\sqrt{s} = 13$ *TeV*, *Eur. Phys. J. C* **84** (2024) 1102 [arXiv:2404.15930] [INSPIRE].

[8] ATLAS collaboration, *Combination and summary of ATLAS dark matter searches interpreted in a 2HDM with a pseudo-scalar mediator using 139* fb^{-1} *of* $\sqrt{s} = 13$ *TeV pp collision data*, *Sci. Bull.* **69** (2024) 3005 [arXiv:2306.00641] [INSPIRE].

[9] FERMI-LAT collaboration, *Fermi-LAT observations of high-energy* γ*-ray emission toward the galactic center*, *Astrophys. J.* **819** (2016) 44 [arXiv:1511.02938] [INSPIRE].

[10] MAGIC and FERMI-LAT collaborations, *Limits to dark matter annihilation cross-section from a combined analysis of MAGIC and Fermi-LAT observations of dwarf satellite galaxies*, *JCAP* **02** (2016) 039 [arXiv:1601.06590] [INSPIRE].

[11] D. Hooper and L. Goodenough, *Dark matter annihilation in the galactic center as seen by the Fermi gamma ray space telescope*, *Phys. Lett. B* **697** (2011) 412 [arXiv:1010.2752] [INSPIRE].

[12] D. Hooper and T. Linden, *On the origin of the gamma rays from the galactic center*, *Phys. Rev. D* **84** (2011) 123005 [arXiv:1110.0006] [INSPIRE].

[13] K.N. Abazajian and M. Kaplinghat, *Detection of a gamma-ray source in the galactic center consistent with extended emission from dark matter annihilation and concentrated astrophysical emission*, *Phys. Rev. D* **86** (2012) 083511 [*Erratum ibid.* **87** (2013) 129902] [arXiv:1207.6047] [INSPIRE].

[14] C. Karwin et al., *Dark matter interpretation of the Fermi-LAT observation toward the galactic center*, *Phys. Rev. D* **95** (2017) 103005 [arXiv:1612.05687] [INSPIRE].

[15] C. Boehm et al., *Extended gamma-ray emission from coy dark matter*, *JCAP* **05** (2014) 009 [arXiv:1401.6458] [INSPIRE].

[16] E. Izaguirre, G. Krnjaic and B. Shuve, *The galactic center excess from the bottom up*, *Phys. Rev. D* **90** (2014) 055002 [arXiv:1404.2018] [INSPIRE].

[17] S. Ipek, D. McKeen and A.E. Nelson, *A renormalizable model for the galactic center gamma ray excess from dark matter annihilation*, *Phys. Rev. D* **90** (2014) 055021 [arXiv:1404.3716] [INSPIRE].

[18] A. Berlin, D. Hooper and S.D. McDermott, *Simplified dark matter models for the galactic center gamma-ray excess*, *Phys. Rev. D* **89** (2014) 115022 [arXiv:1404.0022] [INSPIRE].

[19] C. Arina, E. Del Nobile and P. Panci, *Dark matter with pseudoscalar-mediated interactions explains the DAMA signal and the galactic center excess*, *Phys. Rev. Lett.* **114** (2015) 011301 [arXiv:1406.5542] [INSPIRE].

[20] XENON collaboration, *Constraining the spin-dependent WIMP-nucleon cross sections with XENON1T*, *Phys. Rev. Lett.* **122** (2019) 141301 [arXiv:1902.03234] [INSPIRE].

JHEP06(2026)014

[21] LZ collaboration, *Dark matter search results from 4.2 tonne-years of exposure of the LUX-ZEPLIN (LZ) experiment*, *Phys. Rev. Lett.* **135** (2025) 011802 [arXiv:2410.17036] [INSPIRE].

[22] A. Boveia et al., *Recommendations on presenting LHC searches for missing transverse energy signals using simplified s-channel models of dark matter*, *Phys. Dark Univ.* **27** (2020) 100365 [arXiv:1603.04156] [INSPIRE].

[23] A. Berlin, S. Gori, T. Lin and L.-T. Wang, *Pseudoscalar portal dark matter*, *Phys. Rev. D* **92** (2015) 015005 [arXiv:1502.06000] [INSPIRE].

[24] ATLAS collaboration, *Search for new phenomena in events with an energetic jet and missing transverse momentum in pp collisions at* $\sqrt{s} = 13$ *TeV with the ATLAS detector*, *Phys. Rev. D* **103** (2021) 112006 [arXiv:2102.10874] [INSPIRE].

[25] CMS collaboration, *Search for new particles in events with energetic jets and large missing transverse momentum in proton-proton collisions at* $\sqrt{s} = 13$ *TeV*, *JHEP* **11** (2021) 153 [arXiv:2107.13021] [INSPIRE].

[26] ATLAS collaboration, *Search for dark matter in association with an energetic photon in pp collisions at* $\sqrt{s} = 13$ *TeV with the ATLAS detector*, *JHEP* **02** (2021) 226 [arXiv:2011.05259] [INSPIRE].

[27] CMS collaboration, *Search for new physics in final states with a single photon and missing transverse momentum in proton-proton collisions at* $\sqrt{s} = 13$ *TeV*, *JHEP* **02** (2019) 074 [arXiv:1810.00196] [INSPIRE].

[28] ATLAS collaboration, *Search for associated production of a Z boson with an invisibly decaying Higgs boson or dark matter candidates at* $\sqrt{s} = 13$ *TeV with the ATLAS detector*, *Phys. Lett. B* **829** (2022) 137066 [arXiv:2111.08372] [INSPIRE].

[29] CMS collaboration, *Search for dark matter produced in association with a leptonically decaying Z boson in proton-proton collisions at* $\sqrt{s} = 13$ *TeV*, *Eur. Phys. J. C* **81** (2021) 13 [*Erratum ibid.* **81** (2021) 333] [arXiv:2008.04735] [INSPIRE].

[30] ATLAS collaboration, *Search for dark matter produced in association with a Standard Model Higgs boson decaying into b-quarks using the full run 2 dataset from the ATLAS detector*, *JHEP* **11** (2021) 209 [arXiv:2108.13391] [INSPIRE].

[31] ATLAS collaboration, *Search for dark matter in events with missing transverse momentum and a Higgs boson decaying into two photons in pp collisions at* $\sqrt{s} = 13$ *TeV with the ATLAS detector*, *JHEP* **10** (2021) 013 [arXiv:2104.13240] [INSPIRE].

[32] CMS collaboration, *Search for dark matter particles produced in association with a Higgs boson in proton-proton collisions at* $\sqrt{s} = 13$ *TeV*, *JHEP* **03** (2020) 025 [arXiv:1908.01713] [INSPIRE].

[33] CMS collaboration, *Search for dark matter produced in association with a Higgs boson decaying to a pair of bottom quarks in proton–proton collisions at* $\sqrt{s} = 13$ *TeV*, *Eur. Phys. J. C* **79** (2019) 280 [arXiv:1811.06562] [INSPIRE].

[34] CMS collaboration, *Search for dark matter produced in association with a Higgs boson decaying to* $\gamma\gamma$ *or* $\tau^+\tau^-$ *at* $\sqrt{s} = 13$ *TeV*, *JHEP* **09** (2018) 046 [arXiv:1806.04771] [INSPIRE].

[35] ATLAS collaboration, *Search for dark matter produced in association with a dark Higgs boson decaying into* W^+W^- *in the one-lepton final state at* $\sqrt{s} = 13$ *TeV using* $139\,fb^{-1}$ *of pp collisions recorded with the ATLAS detector*, *JHEP* **07** (2023) 116 [arXiv:2211.07175] [INSPIRE].

JHEP06(2026)014

[36] ATLAS collaboration, *Search for dark matter produced in association with a dark Higgs boson decaying into $W^{\pm}W^{\mp}$ or ZZ in fully hadronic final states from $\sqrt{s} = 13$ TeV pp collisions recorded with the ATLAS detector*, *Phys. Rev. Lett.* **126** (2021) 121802 [arXiv:2010.06548] [INSPIRE].

[37] ATLAS collaboration, *Search for dark matter produced in association with a single top quark and an energetic W boson in $\sqrt{s} = 13$ TeV pp collisions with the ATLAS detector*, *Eur. Phys. J. C* **83** (2023) 603 [arXiv:2211.13138] [INSPIRE].

[38] ATLAS collaboration, *Search for dark matter produced in association with a single top quark in $\sqrt{s} = 13$ TeV pp collisions with the ATLAS detector*, *Eur. Phys. J. C* **81** (2021) 860 [arXiv:2011.09308] [INSPIRE].

[39] CMS collaboration, *Search for dark matter particles produced in association with a top quark pair at $\sqrt{s} = 13$ TeV*, *Phys. Rev. Lett.* **122** (2019) 011803 [arXiv:1807.06522] [INSPIRE].

[40] CMS collaboration, *Search for dark matter produced in association with a single top quark or a top quark pair in proton-proton collisions at $\sqrt{s} = 13$ TeV*, *JHEP* **03** (2019) 141 [arXiv:1901.01553] [INSPIRE].

[41] CMS collaboration, *Measurement of the $B_S^0 \to \mu^+\mu^-$ decay properties and search for the $B^0 \to \mu^+\mu^-$ decay in proton-proton collisions at $\sqrt{s} = 13$ TeV*, *Phys. Lett. B* **842** (2023) 137955 [arXiv:2212.10311] [INSPIRE].

[42] ATLAS collaboration, *Study of the rare decays of B_s^0 and B^0 mesons into muon pairs using data collected during 2015 and 2016 with the ATLAS detector*, *JHEP* **04** (2019) 098 [arXiv:1812.03017] [INSPIRE].

[43] M. Misiak and M. Steinhauser, *Weak radiative decays of the B meson and bounds on $M_{H^\pm}$ in the two-Higgs-doublet model*, *Eur. Phys. J. C* **77** (2017) 201 [arXiv:1702.04571] [INSPIRE].

[44] BELLE collaboration, *Measurement of the inclusive $B \to X_{s+d}\gamma$ branching fraction, photon energy spectrum and HQE parameters*, in the proceedings of the *38th International Conference on High Energy Physics*, Chicago, U.S.A., August 03–10 (2016) [arXiv:1608.02344] [INSPIRE].

[45] H.E. Logan and U. Nierste, *$B_{s,d} \to \ell^+\ell^-$ in a two Higgs doublet model*, *Nucl. Phys. B* **586** (2000) 39 [hep-ph/0004139] [INSPIRE].

[46] M. Misiak et al., *Updated NNLO QCD predictions for the weak radiative B-meson decays*, *Phys. Rev. Lett.* **114** (2015) 221801 [arXiv:1503.01789] [INSPIRE].

[47] CMS collaboration, *Measurement of the $B_s^0 \to \mu^+\mu^-$ branching fraction and search for $B^0 \to \mu^+\mu^-$ with the CMS experiment*, *Phys. Rev. Lett.* **111** (2013) 101804 [arXiv:1307.5025] [INSPIRE].

[48] Y. Nomura and J. Thaler, *Dark matter through the axion portal*, *Phys. Rev. D* **79** (2009) 075008 [arXiv:0810.5397] [INSPIRE].

[49] D. Goncalves, P.A.N. Machado and J.M. No, *Simplified models for dark matter face their consistent completions*, *Phys. Rev. D* **95** (2017) 055027 [arXiv:1611.04593] [INSPIRE].

[50] J.M. No, *Looking through the pseudoscalar portal into dark matter: novel mono-Higgs and mono-Z signatures at the LHC*, *Phys. Rev. D* **93** (2016) 031701 [arXiv:1509.01110] [INSPIRE].

[51] G.C. Branco et al., *Theory and phenomenology of two-Higgs-doublet models*, *Phys. Rept.* **516** (2012) 1 [arXiv:1106.0034] [INSPIRE].

[52] M. Bauer, U. Haisch and F. Kahlhoefer, *Simplified dark matter models with two Higgs doublets: I. Pseudoscalar mediators*, *JHEP* **05** (2017) 138 [arXiv:1701.07427] [INSPIRE].

JHEP06(2026)014

[53] LHC Dark Matter Working Group collaboration, *LHC dark matter working group: next-generation spin-0 dark matter models*, *Phys. Dark Univ.* **27** (2020) 100351 [arXiv:1810.09420] [INSPIRE].

[54] *HEPData record for this analysis*, https://doi.org/10.17182/hepdata.157541 (2025).

[55] CMS collaboration, *The CMS experiment at the CERN LHC*, 2008 *JINST* **3** S08004 [INSPIRE].

[56] CMS collaboration, *Performance of the CMS level-1 trigger in proton-proton collisions at* $\sqrt{s} = 13$ *TeV*, 2020 *JINST* **15** P10017 [arXiv:2006.10165] [INSPIRE].

[57] CMS collaboration, *The CMS trigger system*, 2017 *JINST* **12** P01020 [arXiv:1609.02366] [INSPIRE].

[58] J. Alwall et al., *The automated computation of tree-level and next-to-leading order differential cross sections, and their matching to parton shower simulations*, *JHEP* **07** (2014) 079 [arXiv:1405.0301] [INSPIRE].

[59] R. Frederix and S. Frixione, *Merging meets matching in MC@NLO*, *JHEP* **12** (2012) 061 [arXiv:1209.6215] [INSPIRE].

[60] S. Frixione, P. Nason and C. Oleari, *Matching NLO QCD computations with parton shower simulations: the POWHEG method*, *JHEP* **11** (2007) 070 [arXiv:0709.2092] [INSPIRE].

[61] S. Alioli, P. Nason, C. Oleari and E. Re, *A general framework for implementing NLO calculations in shower Monte Carlo programs: the POWHEG BOX*, *JHEP* **06** (2010) 043 [arXiv:1002.2581] [INSPIRE].

[62] Y. Li and F. Petriello, *Combining QCD and electroweak corrections to dilepton production in FEWZ*, *Phys. Rev. D* **86** (2012) 094034 [arXiv:1208.5967] [INSPIRE].

[63] M. Czakon and A. Mitov, *Top++: a program for the calculation of the top-pair cross-section at hadron colliders*, *Comput. Phys. Commun.* **185** (2014) 2930 [arXiv:1112.5675] [INSPIRE].

[64] N. Kidonakis, *Two-loop soft anomalous dimensions for single top quark associated production with a* W^- *or* H^-, *Phys. Rev. D* **82** (2010) 054018 [arXiv:1005.4451] [INSPIRE].

[65] J.M. Campbell, R.K. Ellis and C. Williams, *Vector boson pair production at the LHC*, *JHEP* **07** (2011) 018 [arXiv:1105.0020] [INSPIRE].

[66] M. Czakon et al., *Top-pair production at the LHC through NNLO QCD and NLO EW*, *JHEP* **10** (2017) 186 [arXiv:1705.04105] [INSPIRE].

[67] M. Grazzini, S. Kallweit and M. Wiesemann, *Fully differential NNLO computations with MATRIX*, *Eur. Phys. J. C* **78** (2018) 537 [arXiv:1711.06631] [INSPIRE].

[68] CMS collaboration, *Measurement of the inclusive and differential WZ production cross sections, polarization angles, and triple gauge couplings in pp collisions at* $\sqrt{s} = 13$ *TeV*, *JHEP* **07** (2022) 032 [arXiv:2110.11231] [INSPIRE].

[69] NNPDF collaboration, *Parton distributions from high-precision collider data*, *Eur. Phys. J. C* **77** (2017) 663 [arXiv:1706.00428] [INSPIRE].

[70] T. Sjöstrand et al., *An introduction to PYTHIA 8.2*, *Comput. Phys. Commun.* **191** (2015) 159 [arXiv:1410.3012] [INSPIRE].

[71] CMS collaboration, *Extraction and validation of a new set of CMS PYTHIA8 tunes from underlying-event measurements*, *Eur. Phys. J. C* **80** (2020) 4 [arXiv:1903.12179] [INSPIRE].

[72] GEANT4 collaboration, *GEANT4 — a simulation toolkit*, *Nucl. Instrum. Meth. A* **506** (2003) 250 [INSPIRE].

JHEP06(2026)014

[73] CMS collaboration, *Particle-flow reconstruction and global event description with the CMS detector*, 2017 *JINST* **12** P10003 [arXiv:1706.04965] [INSPIRE].

[74] D. Contardo et al., *Technical proposal for the phase-II upgrade of the CMS detector*, CERN-LHCC-2015-010 (2015) [DOI:10.17181/CERN.VU8I.D59J] [INSPIRE].

[75] CMS collaboration, *Electron and photon reconstruction and identification with the CMS experiment at the CERN LHC*, 2021 *JINST* **16** P05014 [arXiv:2012.06888] [INSPIRE].

[76] CMS collaboration, *Performance of the CMS muon detector and muon reconstruction with proton-proton collisions at* $\sqrt{s} = 13$ *TeV*, 2018 *JINST* **13** P06015 [arXiv:1804.04528] [INSPIRE].

[77] M. Cacciari, G.P. Salam and G. Soyez, *The anti-*k_t *jet clustering algorithm*, *JHEP* **04** (2008) 063 [arXiv:0802.1189] [INSPIRE].

[78] M. Cacciari, G.P. Salam and G. Soyez, *FastJet user manual*, *Eur. Phys. J. C* **72** (2012) 1896 [arXiv:1111.6097] [INSPIRE].

[79] M. Cacciari and G.P. Salam, *Dispelling the* N^3 *myth for the* k_t *jet-finder*, *Phys. Lett. B* **641** (2006) 57 [hep-ph/0512210] [INSPIRE].

[80] CMS collaboration, *Jet energy scale and resolution in the CMS experiment in pp collisions at 8 TeV*, 2017 *JINST* **12** P02014 [arXiv:1607.03663] [INSPIRE].

[81] CMS collaboration, *Pileup mitigation at CMS in 13 TeV data*, 2020 *JINST* **15** P09018 [arXiv:2003.00503] [INSPIRE].

[82] CMS collaboration, *Identification of heavy-flavour jets with the CMS detector in pp collisions at 13 TeV*, 2018 *JINST* **13** P05011 [arXiv:1712.07158] [INSPIRE].

[83] CMS collaboration, *Performance of missing transverse momentum reconstruction in proton-proton collisions at* $\sqrt{s} = 13$ *TeV using the CMS detector*, 2019 *JINST* **14** P07004 [arXiv:1903.06078] [INSPIRE].

[84] Particle Data Group collaboration, *Review of particle physics*, *Phys. Rev. D* **110** (2024) 030001 [INSPIRE].

[85] C.G. Lester and D.J. Summers, *Measuring masses of semiinvisibly decaying particles pair produced at hadron colliders*, *Phys. Lett. B* **463** (1999) 99 [hep-ph/9906349] [INSPIRE].

[86] L. Sonnenschein, *Analytical solution of* $t\bar{t}$ *dilepton equations*, *Phys. Rev. D* **73** (2006) 054015 [*Erratum ibid.* **78** (2008) 079902] [hep-ph/0603011] [INSPIRE].

[87] A. Paszke et al., *PyTorch: an imperative style, high-performance deep learning library*, arXiv:1912.01703 [INSPIRE].

[88] C.G. Lester and B. Nachman, *Bisection-based asymmetric* M_{T2} *computation: a higher precision calculator than existing symmetric methods*, *JHEP* **03** (2015) 100 [arXiv:1411.4312] [INSPIRE].

[89] L. Breiman, *Random forests*, *Mach. Learn.* **45** (2001) 5 [INSPIRE].

[90] J. Butterworth et al., *PDF4LHC recommendations for LHC run II*, *J. Phys. G* **43** (2016) 023001 [arXiv:1510.03865] [INSPIRE].

[91] A. Accardi et al., *A critical appraisal and evaluation of modern PDFs*, *Eur. Phys. J. C* **76** (2016) 471 [arXiv:1603.08906] [INSPIRE].

[92] R.J. Barlow and C. Beeston, *Fitting using finite Monte Carlo samples*, *Comput. Phys. Commun.* **77** (1993) 219 [INSPIRE].

JHEP06(2026)014

[93] CMS collaboration, *Measurement of the $t\bar{t}$ production cross section, the top quark mass, and the strong coupling constant using dilepton events in pp collisions at $\sqrt{s} = 13$ TeV*, *Eur. Phys. J. C* **79** (2019) 368 [arXiv:1812.10505] [INSPIRE].

[94] CMS collaboration, *Measurement of the inelastic proton-proton cross section at $\sqrt{s} = 13$ TeV*, *JHEP* **07** (2018) 161 [arXiv:1802.02613] [INSPIRE].

[95] CMS collaboration, *Precision luminosity measurement in proton-proton collisions at $\sqrt{s} = 13$ TeV in 2015 and 2016 at CMS*, *Eur. Phys. J. C* **81** (2021) 800 [arXiv:2104.01927] [INSPIRE].

[96] CMS collaboration, *CMS luminosity measurement for the 2017 data-taking period at $\sqrt{s} = 13$ TeV*, CMS-PAS-LUM-17-004 (2018) [INSPIRE].

[97] CMS collaboration, *CMS luminosity measurement for the 2018 data-taking period at $\sqrt{s} = 13$ TeV*, CMS-PAS-LUM-18-002 (2019) [INSPIRE].

[98] CMS collaboration, *The CMS statistical analysis and combination tool: Combine*, *Comput. Softw. Big Sci.* **8** (2024) 19 [arXiv:2404.06614] [INSPIRE].

[99] F. Cascioli et al., *ZZ production at hadron colliders in NNLO QCD*, *Phys. Lett. B* **735** (2014) 311 [arXiv:1405.2219] [INSPIRE].

[100] M. Grazzini, S. Kallweit, D. Rathlev and M. Wiesemann, *$W^{\pm}Z$ production at the LHC: fiducial cross sections and distributions in NNLO QCD*, *JHEP* **05** (2017) 139 [arXiv:1703.09065] [INSPIRE].

[101] M. Grazzini, S. Kallweit, M. Wiesemann and J.Y. Yook, *ZZ production at the LHC: NLO QCD corrections to the loop-induced gluon fusion channel*, *JHEP* **03** (2019) 070 [arXiv:1811.09593] [INSPIRE].

[102] A.L. Read, *Presentation of search results: the CL_s technique*, *J. Phys. G* **28** (2002) 2693 [INSPIRE].

[103] G. Cowan, K. Cranmer, E. Gross and O. Vitells, *Asymptotic formulae for likelihood-based tests of new physics*, *Eur. Phys. J. C* **71** (2011) 1554 [*Erratum ibid.* **73** (2013) 2501] [arXiv:1007.1727] [INSPIRE].

[104] ATLAS collaboration, *Search for new phenomena using the invariant mass distribution of same-flavour opposite-sign dilepton pairs in events with missing transverse momentum in $\sqrt{s} = 13$ TeV pp collisions with the ATLAS detector*, *Eur. Phys. J. C* **78** (2018) 625 [arXiv:1805.11381] [INSPIRE].

[105] CMS collaboration, *Search for supersymmetry in final states with two or three soft leptons and missing transverse momentum in proton-proton collisions at $\sqrt{s} = 13$ TeV*, *JHEP* **04** (2022) 091 [arXiv:2111.06296] [INSPIRE].

[106] J. Alwall et al., *Computing decay rates for new physics theories with FeynRules and MadGraph 5_aMC@NLO*, *Comput. Phys. Commun.* **197** (2015) 312 [arXiv:1402.1178] [INSPIRE].

[107] M. Backovic, K. Kong and M. McCaskey, *MadDM v.1.0: computation of dark matter relic abundance using MadGraph5*, *Physics of the Dark Universe* **5-6** (2014) 18 [arXiv:1308.4955] [INSPIRE].

[108] PLANCK collaboration, *Planck 2015 results. XIII. Cosmological parameters*, *Astron. Astrophys.* **594** (2016) A13 [arXiv:1502.01589] [INSPIRE].

[109] G. Steigman, B. Dasgupta and J.F. Beacom, *Precise relic WIMP abundance and its impact on searches for dark matter annihilation*, *Phys. Rev. D* **86** (2012) 023506 [arXiv:1204.3622] [INSPIRE].

JHEP06(2026)014

The CMS collaboration

V. Chekhovsky[1], A. Hayrapetyan[1], V. Makarenko[1], A. Tumasyan[1,a], W. Adam[2], J.W. Andrejkovic[2], L. Benato[2], T. Bergauer[2], K. Damanakis[2], M. Dragicevic[2], C. Giordano[2], P.S. Hussain[2], M. Jeitler[2,b], N. Krammer[2], A. Li[2], D. Liko[2], I. Mikulec[2], J. Schieck[2,b], D. Schwarz[2], R. Schöfbeck[2,b], M. Sonawane[2], W. Waltenberger[2], C.-E. Wulz[2,b], T. Janssen[3], H. Kwon[3], T. Van Laer[3], P. Van Mechelen[3], J. Bierkens[4], N. Breugelmans[4], J. D'Hondt[4], S. Dansana[4], A. De Moor[4], M. Delcourt[4], F. Heyen[4], Y. Hong[4], S. Lowette[4], I. Makarenko[4], D. Müller[4], S. Tavernier[4], M. Tytgat[4,c], G.P. Van Onsem[4], S. Van Putte[4], D. Vannerom[4], B. Bilin[5], B. Clerbaux[5], A.K. Das[5], I. De Bruyn[5], G. De Lentdecker[5], H. Evard[5], L. Favart[5], P. Gianneios[5], A. Khalilzadeh[5], F.A. Khan[5], A. Malara[5], M.A. Shahzad[5], L. Thomas[5], M. Vanden Bemden[5], C. Vander Velde[5], P. Vanlaer[5], F. Zhang[5], M. De Coen[6], D. Dobur[6], G. Gokbulut[6], J. Knolle[6], L. Lambrecht[6], D. Marckx[6], K. Skovpen[6], N. Van Den Bossche[6], J. van der Linden[6], J. Vandenbroeck[6], L. Wezenbeek[6], S. Bein[7], A. Benecke[7], A. Bethani[7], G. Bruno[7], A. Cappati[7], J. De Favereau De Jeneret[7], C. Delaere[7], A. Giammanco[7], A.O. Guzel[7], Sa. Jain[7], V. Lemaitre[7], J. Lidrych[7], P. Mastrapasqua[7], S. Turkcapar[7], G.A. Alves[8], E. Coelho[8], G. Correia Silva[8], C. Hensel[8], T. Menezes De Oliveira[8], C. Mora Herrera[8,d], P. Rebello Teles[8], M. Soeiro[8], E.J. Tonelli Manganote[8,e], A. Vilela Pereira[8,d], W.L. Aldá Júnior[9], M. Barroso Ferreira Filho[9], H. Brandao Malbouisson[9], W. Carvalho[9], J. Chinellato[9,f], E.M. Da Costa[9], G.G. Da Silveira[9,g], D. De Jesus Damiao[9], S. Fonseca De Souza[9], R. Gomes De Souza[9], S. S. Jesus[9], T. Laux Kuhn[9,g], M. Macedo[9], K. Mota Amarilo[9], L. Mundim[9], H. Nogima[9], J.P. Pinheiro[9], A. Santoro[9], A. Sznajder[9], M. Thiel[9], C.A. Bernardes[10,g], L. Calligaris[10], E.M. Gregores[10], I. Maietto Silverio[10], P.G. Mercadante[10], S.F. Novaes[10], B. Orzari[10], Sandra S. Padula[10], V. Scheurer[10], T.R. Fernandez Perez Tomei[10], A. Aleksandrov[11], G. Antchev[11], R. Hadjiiska[11], P. Iaydjiev[11], M. Misheva[11], M. Shopova[11], G. Sultanov[11], A. Dimitrov[12], L. Litov[12], B. Pavlov[12], P. Petkov[12], A. Petrov[12], E. Shumka[12], S. Keshri[13], D. Laroze[13], S. Thakur[13], T. Cheng[14], Q. Guo[14], T. Javaid[14], L. Yuan[14], Z. Hu[15], Z. Liang[15], J. Liu[15], G.M. Chen[16,h], H.S. Chen[16,h], M. Chen[16,h], Q. Hou[16], F. Iemmi[16], C.H. Jiang[16], A. Kapoor[16,i], H. Liao[16], Z.-A. Liu[16,j], R. Sharma[16,k], J.N. Song[16,j], J. Tao[16], C. Wang[16,h], J. Wang[16], H. Zhang[16], J. Zhao[16], A. Agapitos[17], Y. Ban[17], A. Carvalho Antunes De Oliveira[17], S. Deng[17], B. Guo[17], C. Jiang[17], A. Levin[17], C. Li[17], Q. Li[17], Y. Mao[17], S. Qian[17], S.J. Qian[17], X. Qin[17], X. Sun[17], D. Wang[17], H. Yang[17], Y. Zhao[17], C. Zhou[17], S. Yang[18], Z. You[19], K. Jaffel[20], N. Lu[20], G. Bauer[21,l], B. Li[21,m], H. Wang[21], K. Yi[21,n], J. Zhang[21], Y. Li[22], Z. Lin[23], C. Lu[23], M. Xiao[23], C. Avila[24], D.A. Barbosa Trujillo[24], A. Cabrera[24], C. Florez[24], J. Fraga[24], J.A. Reyes Vega[24], J. Jaramillo[25], C. Rendón[25], M. Rodriguez[25], A.A. Ruales Barbosa[25], J.D. Ruiz Alvarez[25], D. Giljanovic[26], N. Godinovic[26], D. Lelas[26], A. Sculac[26], M. Kovac[27], A. Petkovic[27], T. Sculac[27], P. Bargassa[28], V. Brigljevic[28], B.K. Chitroda[28], D. Ferencek[28], K. Jakovcic[28], A. Starodumov[28], T. Susa[28], A. Attikis[29], K. Christoforou[29], A. Hadjiagapiou[29], C. Leonidou[29], J. Mousa[29], C. Nicolaou[29], L. Paizanos[29], F. Ptochos[29], P.A. Razis[29], H. Rykaczewski[29], H. Saka[29], A. Stepennov[29], M. Finger[30], M. Finger Jr.[30], A. Kveton[30], E. Ayala[31], E. Carrera Jarrin[32], H. Abdalla[33,o], R. Aly[33,p], Y. Assran[33,q,r],

JHEP06(2026)014

M.A. Mahmoud[34], M. Abdullah Al-Mashad[34], K. Ehataht[35], M. Kadastik[35], T. Lange[35], C. Nielsen[35], J. Pata[35], M. Raidal[35], L. Tani[35], C. Veelken[35], K. Osterberg[36], M. Voutilainen[36], N. Bin Norjoharuddeen[37], E. Brücken[37], F. Garcia[37], P. Inkaew[37], K.T.S. Kallonen[37], T. Lampén[37], K. Lassila-Perini[37], S. Lehti[37], T. Lindén[37], M. Myllymäki[37], M.m. Rantanen[37], S. Saariokari[37], J. Tuominiemi[37], H. Kirschenmann[38], P. Luukka[38], H. Petrow[38], M. Besancon[39], F. Couderc[39], M. Dejardin[39], D. Denegri[39], J.L. Faure[39], F. Ferri[39], S. Ganjour[39], P. Gras[39], G. Hamel de Monchenault[39], M. Kumar[39], V. Lohezic[39], J. Malcles[39], F. Orlandi[39], L. Portales[39], A. Rosowsky[39], M.Ö. Sahin[39], A. Savoy-Navarro[39,s], P. Simkina[39], M. Titov[39], M. Tornago[39], F. Beaudette[40], G. Boldrini[40], P. Busson[40], C. Charlot[40], M. Chiusi[40], T.D. Cuisset[40], F. Damas[40], O. Davignon[40], A. De Wit[40], I.T. Ehle[40], B.A. Fontana Santos Alves[40], S. Ghosh[40], A. Gilbert[40], R. Granier de Cassagnac[40], L. Kalipoliti[40], G. Liu[40], M. Manoni[40], M. Nguyen[40], S. Obraztsov[40], C. Ochando[40], R. Salerno[40], J.B. Sauvan[40], Y. Sirois[40], G. Sokmen[40], L. Urda Gómez[40], E. Vernazza[40], A. Zabi[40], A. Zghiche[40], J.-L. Agram[41,t], J. Andrea[41], D. Bloch[41], J.-M. Brom[41], E.C. Chabert[41], C. Collard[41], S. Falke[41], U. Goerlach[41], R. Haeberle[41], A.-C. Le Bihan[41], M. Meena[41], O. Poncet[41], G. Saha[41], M.A. Sessini[41], P. Van Hove[41], P. Vaucelle[41], A. Di Florio[42], D. Amram[43], S. Beauceron[43], B. Blancon[43], G. Boudoul[43], N. Chanon[43], D. Contardo[43], P. Depasse[43], C. Dozen[43,u], H. El Mamouni[43], J. Fay[43], S. Gascon[43], M. Gouzevitch[43], C. Greenberg[43], G. Grenier[43], B. Ille[43], E. Jourd'huy[43], I.B. Laktineh[43], M. Lethuillier[43], L. Mirabito[43], S. Perries[43], A. Purohit[43], M. Vander Donckt[43], P. Verdier[43], J. Xiao[43], A. Khvedelidze[44,v], I. Lomidze[44], Z. Tsamalaidze[44,v], V. Botta[45], S. Consuegra Rodríguez[45], L. Feld[45], K. Klein[45], M. Lipinski[45], D. Meuser[45], V. Oppenländer[45], A. Pauls[45], D. Pérez Adán[45], N. Röwert[45], M. Teroerde[45], S. Diekmann[46], A. Dodonova[46], N. Eich[46], D. Eliseev[46], F. Engelke[46], J. Erdmann[46], M. Erdmann[46], B. Fischer[46], T. Hebbeker[46], K. Hoepfner[46], F. Ivone[46], A. Jung[46], N. Kumar[46], M.y. Lee[46], F. Mausolf[46], M. Merschmeyer[46], A. Meyer[46], F. Nowotny[46], A. Pozdnyakov[46], Y. Rath[46], W. Redjeb[46], F. Rehm[46], H. Reithler[46], V. Sarkisovi[46], A. Schmidt[46], C. Seth[46], A. Sharma[46], J.L. Spah[46], F. Torres Da Silva De Araujo[46,w], S. Wiedenbeck[46], S. Zaleski[46], C. Dziwok[47], G. Flügge[47], T. Kress[47], A. Nowack[47], O. Pooth[47], A. Stahl[47], T. Ziemons[47], A. Zotz[47], H. Aarup Petersen[48], M. Aldaya Martin[48], J. Alimena[48], S. Amoroso[48], Y. An[48], J. Bach[48], S. Baxter[48], M. Bayatmakou[48], H. Becerril Gonzalez[48], O. Behnke[48], A. Belvedere[48], F. Blekman[48,x], K. Borras[48,y], A. Campbell[48], S. Chatterjee[48], F. Colombina[48], M. De Silva[48], G. Eckerlin[48], D. Eckstein[48], E. Gallo[48,x], A. Geiser[48], V. Guglielmi[48], M. Guthoff[48], A. Hinzmann[48], L. Jeppe[48], B. Kaech[48], M. Kasemann[48], C. Kleinwort[48], R. Kogler[48], M. Komm[48], D. Krücker[48], W. Lange[48], D. Leyva Pernia[48], K. Lipka[48,z], W. Lohmann[48,aa], F. Lorkowski[48], R. Mankel[48], I.-A. Melzer-Pellmann[48], M. Mendizabal Morentin[48], A.B. Meyer[48], G. Milella[48], K. Moral Figueroa[48], A. Mussgiller[48], L.P. Nair[48], J. Niedziela[48], A. Nürnberg[48], J. Park[48], E. Ranken[48], A. Raspereza[48], D. Rastorguev[48], L. Rygaard[48], J. Rübenach[48], M. Scham[48,ab,ac], S. Schnake[48,y], C. Schwanenberger[48,x], P. Schütze[48], D. Selivanova[48], K. Sharko[48], M. Shchedrolosiev[48], D. Stafford[48], F. Vazzoler[48], A. Ventura Barroso[48], R. Walsh[48], D. Wang[48], Q. Wang[48], K. Wichmann[48], L. Wiens[48,y], C. Wissing[48],

JHEP06(2026)014

Y. Yang[48], S. Zakharov[48], A. Zimermmane Castro Santos[48], A. Albrecht[49], S. Albrecht[49], M. Antonello[49], S. Bollweg[49], M. Bonanomi[49], P. Connor[49], K. El Morabit[49], Y. Fischer[49], E. Garutti[49], A. Grohsjean[49], J. Haller[49], D. Hundhausen[49], H.R. Jabusch[49], G. Kasieczka[49], P. Keicher[49], R. Klanner[49], W. Korcari[49], T. Kramer[49], C.c. Kuo[49], V. Kutzner[49], F. Labe[49], J. Lange[49], A. Lobanov[49], C. Matthies[49], L. Moureaux[49], M. Mrowietz[49], A. Nigamova[49], K. Nikolopoulos[49], Y. Nissan[49], A. Paasch[49], K.J. Pena Rodriguez[49], T. Quadfasel[49], B. Raciti[49], M. Rieger[49], D. Savoiu[49], J. Schindler[49], P. Schleper[49], M. Schröder[49], J. Schwandt[49], M. Sommerhalder[49], H. Stadie[49], G. Steinbrück[49], A. Tews[49], R. Ward[49], B. Wiederspan[49], M. Wolf[49], S. Brommer[50], E. Butz[50], Y.M. Chen[50], T. Chwalek[50], A. Dierlamm[50], G.G. Dincer[50], U. Elicabuk[50], N. Faltermann[50], M. Giffels[50], A. Gottmann[50], F. Hartmann[50,ad], R. Hofsaess[50], M. Horzela[50], U. Husemann[50], J. Kieseler[50], M. Klute[50], O. Lavoryk[50], J.M. Lawhorn[50], M. Link[50], A. Lintuluoto[50], S. Maier[50], M. Mormile[50], Th. Müller[50], M. Neukum[50], M. Oh[50], E. Pfeffer[50], M. Presilla[50], G. Quast[50], K. Rabbertz[50], B. Regnery[50], R. Schmieder[50], N. Shadskiy[50], I. Shvetsov[50], H.J. Simonis[50], L. Sowa[50], L. Stockmeier[50], K. Tauqeer[50], M. Toms[50], B. Topko[50], N. Trevisani[50], T. Voigtländer[50], R.F. Von Cube[50], J. Von Den Driesch[50], M. Wassmer[50], S. Wieland[50], F. Wittig[50], R. Wolf[50], X. Zuo[50], G. Anagnostou[51], G. Daskalakis[51], A. Kyriakis[51], A. Papadopoulos[51,ad], A. Stakia[51], G. Melachroinos[52], Z. Painesis[52], I. Paraskevas[52], N. Saoulidou[52], K. Theofilatos[52], E. Tziaferi[52], K. Vellidis[52], I. Zisopoulos[52], T. Chatzistavrou[53], G. Karapostoli[53], K. Kousouris[53], E. Siamarkou[53], G. Tsipolitis[53], I. Bestintzanos[54], I. Evangelou[54], C. Foudas[54], C. Kamtsikis[54], P. Katsoulis[54], P. Kokkas[54], P.G. Kosmoglou Kioseoglou[54], N. Manthos[54], I. Papadopoulos[54], J. Strologas[54], C. Hajdu[55], D. Horvath[55,ae,af], K. Márton[55], A.J. Rádl[55,ag], F. Sikler[55], V. Veszpremi[55], M. Csanád[56], K. Farkas[56], A. Fehérkuti[56,ah], M.M.A. Gadallah[56,ai], Á. Kadlecsik[56], G. Pásztor[56], G.I. Veres[56], B. Ujvari[57], G. Zilizi[57], G. Bencze[58], S. Czellar[58], J. Molnar[58], Z. Szillasi[58], T. Csorgo[59,ah], F. Nemes[59,ah], T. Novak[59], S. Bansal[60], S.B. Beri[60], V. Bhatnagar[60], G. Chaudhary[60], S. Chauhan[60], N. Dhingra[60,aj], A. Kaur[60], A. Kaur[60], H. Kaur[60], M. Kaur[60], S. Kumar[60], T. Sheokand[60], J.B. Singh[60], A. Singla[60], A. Bhardwaj[61], A. Chhetri[61], B.C. Choudhary[61], A. Kumar[61], A. Kumar[61], M. Naimuddin[61], S. Saumya[61], K. Ranjan[61], M.K. Saini[61], S. Mukherjee[62], S. Baradia[63], S. Barman[63,ak], S. Bhattacharya[63], S. Das Gupta[63], S. Dutta[63], S. Dutta[63], S. Sarkar[63], M.M. Ameen[64], P.K. Behera[64], S.C. Behera[64], S. Chatterjee[64], G. Dash[64], A. Dattamunsi[64], P. Jana[64], P. Kalbhor[64], S. Kamble[64], J.R. Komaragiri[64,al], D. Kumar[64,al], T. Mishra[64], B. Parida[64,am], P.R. Pujahari[64], N.R. Saha[64], A.K. Sikdar[64], R.K. Singh[64], P. Verma[64], S. Verma[64], A. Vijay[64], S. Dugad[65], G.B. Mohanty[65], M. Shelake[65], P. Suryadevara[65], A. Bala[66], S. Banerjee[66], S. Bhowmik[66,an], R.M. Chatterjee[66], M. Guchait[66], Sh. Jain[66], A. Jaiswal[66], B.M. Joshi[66], S. Kumar[66], G. Majumder[66], K. Mazumdar[66], S. Parolia[66], A. Thachayath[66], S. Bahinipati[67,ao], C. Kar[67], D. Maity[67,ap], P. Mal[67], K. Naskar[67,ap], A. Nayak[67,ap], S. Nayak[67], K. Pal[67], R. Raturi[67], P. Sadangi[67], S.K. Swain[67], S. Varghese[67,ap], D. Vats[67,ap], S. Acharya[68,aq], A. Alpana[68], S. Dube[68], B. Gomber[68,aq], P. Hazarika[68], B. Kansal[68], A. Laha[68], B. Sahu[68,aq], S. Sharma[68], K.Y. Vaish[68], H. Bakhshiansohi[69,ar],

JHEP06(2026)014

A. Jafari[69,as], M. Zeinali[69,at], S. Bashiri[70], S. Chenarani[70,au], S.M. Etesami[70], Y. Hosseini[70], M. Khakzad[70], E. Khazaie[70], M. Mohammadi Najafabadi[70], S. Tizchang[70,av], M. Felcini[71], M. Grunewald[71], M. Abbrescia[72a,72b], M. Barbieri[72a,72b], M. Buonsante[72a,72b], A. Colaleo[72a,72b], D. Creanza[72a,72c], B. D'Anzi[72a,72b], N. De Filippis[72a,72c], M. De Palma[72a,72b], W. Elmetenawee[72a,72b,p], N. Ferrara[72a,72b], L. Fiore[72a], G. Iaselli[72a,72c], L. Longo[72a], M. Louka[72a,72b], G. Maggi[72a,72c], M. Maggi[72a], I. Margjeka[72a], V. Mastrapasqua[72a,72b], S. My[72a,72b], S. Nuzzo[72a,72b], A. Pellecchia[72a,72b], A. Pompili[72a,72b], G. Pugliese[72a,72c], R. Radogna[72a,72b], D. Ramos[72a], A. Ranieri[72a], L. Silvestris[72a], F.M. Simone[72a,72c], A. Stamerra[72a,72b], Ü. Sözbilir[72a], D. Troiano[72a,72b], R. Venditti[72a,72b], P. Verwilligen[72a], A. Zaza[72a,72b], G. Abbiendi[73a], C. Battilana[73a,73b], D. Bonacorsi[73a,73b], P. Capiluppi[73a,73b], A. Castro[73a,73b,†], F.R. Cavallo[73a], M. Cuffiani[73a,73b], G.M. Dallavalle[73a], T. Diotalevi[73a,73b], F. Fabbri[73a], A. Fanfani[73a,73b], D. Fasanella[73a], P. Giacomelli[73a], L. Giommi[73a,73b], C. Grandi[73a], L. Guiducci[73a,73b], S. Lo Meo[73a,aw], M. Lorusso[73a,73b], L. Lunerti[73a], S. Marcellini[73a], G. Masetti[73a], F.L. Navarria[73a,73b], G. Paggi[73a,73b], A. Perrotta[73a], F. Primavera[73a,73b], A.M. Rossi[73a,73b], S. Rossi Tisbeni[73a,73b], T. Rovelli[73a,73b], G.P. Siroli[73a,73b], S. Costa[74a,74b,ax], A. Di Mattia[74a], A. Lapertosa[74a], R. Potenza[74a,74b], A. Tricomi[74a,74b,ax], J. Altork[75a], P. Assiouras[75a], G. Barbagli[75a], G. Bardelli[75a,75b], M. Bartolini[75a,75b], B. Camaiani[75a,75b], A. Cassese[75a], R. Ceccarelli[75a], V. Ciulli[75a,75b], C. Civinini[75a], R. D'Alessandro[75a,75b], L. Damenti[75a,75b], E. Focardi[75a,75b], T. Kello[75a], G. Latino[75a,75b], P. Lenzi[75a,75b], M. Lizzo[75a], M. Meschini[75a], S. Paoletti[75a], A. Papanastassiou[75a,75b], G. Sguazzoni[75a], L. Viliani[75a], L. Benussi[76], S. Bianco[76], S. Meola[76,ay], D. Piccolo[76], M. Alves Gallo Pereira[77a], F. Ferro[77a], E. Robutti[77a], S. Tosi[77a,77b], A. Benaglia[78a], F. Brivio[78a], F. Cetorelli[78a,78b], F. De Guio[78a,78b], M.E. Dinardo[78a,78b], P. Dini[78a], S. Gennai[78a], R. Gerosa[78a,78b], A. Ghezzi[78a,78b], P. Govoni[78a,78b], L. Guzzi[78a], G. Lavizzari[78a,78b], M.T. Lucchini[78a,78b], M. Malberti[78a], S. Malvezzi[78a], A. Massironi[78a], D. Menasce[78a], L. Moroni[78a], M. Paganoni[78a,78b], S. Palluotto[78a,78b], D. Pedrini[78a], A. Perego[78a,78b], B.S. Pinolini[78a], G. Pizzati[78a,78b], S. Ragazzi[78a,78b], T. Tabarelli de Fatis[78a,78b], S. Buontempo[79a], A. Cagnotta[79a,79b], F. Carnevali[79a,79b], N. Cavallo[79a,79c], C. Di Fraia[79a], F. Fabozzi[79a,79c], A.O.M. Iorio[79a,79b], L. Lista[79a,79b,az], P. Paolucci[79a,ad], B. Rossi[79a], R. Ardino[80a], P. Azzi[80a], N. Bacchetta[80a,ba], D. Bisello[80a,80b], P. Bortignon[80a], G. Bortolato[80a,80b], A.C.M. Bulla[80a], R. Carlin[80a,80b], T. Dorigo[80a,bb], F. Gasparini[80a,80b], U. Gasparini[80a,80b], S. Giorgetti[80a], E. Lusiani[80a], M. Margoni[80a,80b], G. Maron[80a,bc], A.T. Meneguzzo[80a,80b], J. Pazzini[80a,80b], P. Ronchese[80a,80b], R. Rossin[80a,80b], F. Simonetto[80a,80b], M. Tosi[80a,80b], A. Triossi[80a,80b], S. Ventura[80a], M. Zanetti[80a,80b], P. Zotto[80a,80b], A. Zucchetta[80a,80b], G. Zumerle[80a,80b], A. Braghieri[81a], S. Calzaferri[81a], D. Fiorina[81a], P. Montagna[81a,81b], M. Pelliccioni[81a], V. Re[81a], C. Riccardi[81a,81b], P. Salvini[81a], I. Vai[81a,81b], P. Vitulo[81a,81b], S. Ajmal[82a,82b], M.E. Ascioti[82a,82b], G.M. Bilei[82a], C. Carrivale[82a,82b], D. Ciangottini[82a,82b], L. Fanò[82a,82b], V. Mariani[82a,82b], M. Menichelli[82a], F. Moscatelli[82a,bd], A. Rossi[82a,82b], A. Santocchia[82a,82b], D. Spiga[82a], T. Tedeschi[82a,82b], C. Aimè[83a,83b], C.A. Alexe[83a,83c], P. Asenov[83a,83b], P. Azzurri[83a], G. Bagliesi[83a], R. Bhattacharya[83a], L. Bianchini[83a,83b], T. Boccali[83a], E. Bossini[83a], D. Bruschini[83a,83c], R. Castaldi[83a], F. Cattafesta[83a,83c],

JHEP06(2026)014

M.A. Ciocci[83a,83b], M. Cipriani[83a,83b], V. D'Amante[83a,83d], R. Dell'Orso[83a], S. Donato[83a,83b], R. Forti[83a,83b], A. Giassi[83a], F. Ligabue[83a,83c], A.C. Marini[83a,83b], D. Matos Figueiredo[83a], A. Messineo[83a,83b], S. Mishra[83a], V.K. Muraleedharan Nair Bindhu[83a,83b], M. Musich[83a,83b], S. Nandan[83a], F. Palla[83a], M. Riggirello[83a,83c], A. Rizzi[83a,83b], G. Rolandi[83a,83c], S. Roy Chowdhury[83a,an], T. Sarkar[83a], A. Scribano[83a], P. Spagnolo[83a], F. Tenchini[83a,83b], R. Tenchini[83a], G. Tonelli[83a,83b], N. Turini[83a,83d], F. Vaselli[83a,83c], A. Venturi[83a], P.G. Verdini[83a], P. Akrap[84a,84b], C. Basile[84a,84b], F. Cavallari[84a], L. Cunqueiro Mendez[84a,84b], F. De Riggi[84a,84b], D. Del Re[84a,84b], E. Di Marco[84a,84b], M. Diemoz[84a], F. Errico[84a,84b], L. Frosina[84a,84b], R. Gargiulo[84a,84b], B. Harikrishnan[84a,84b], F. Lombardi[84a,84b], E. Longo[84a,84b], L. Martikainen[84a,84b], J. Mijuskovic[84a,84b], G. Organtini[84a,84b], N. Palmeri[84a,84b], F. Pandolfi[84a], R. Paramatti[84a,84b], C. Quaranta[84a,84b], S. Rahatlou[84a,84b], C. Rovelli[84a], F. Santanastasio[84a,84b], L. Soffi[84a], V. Vladimirov[84a,84b], N. Amapane[85a,85b], R. Arcidiacono[85a,85c], S. Argiro[85a,85b], M. Arneodo[85a,85c], N. Bartosik[85a,85c], R. Bellan[85a,85b], C. Biino[85a], C. Borca[85a,85b], N. Cartiglia[85a], M. Costa[85a,85b], R. Covarelli[85a,85b], N. Demaria[85a], M. Ferrero[85a], L. Finco[85a], M. Grippo[85a,85b], B. Kiani[85a,85b], F. Legger[85a], F. Luongo[85a,85b], C. Mariotti[85a], L. Markovic[85a,85b], S. Maselli[85a], A. Mecca[85a,85b], L. Menzio[85a,85b], P. Meridiani[85a], E. Migliore[85a,85b], M. Monteno[85a], R. Mulargia[85a], M.M. Obertino[85a,85b], G. Ortona[85a], L. Pacher[85a,85b], N. Pastrone[85a], M. Ruspa[85a,85c], F. Siviero[85a,85b], V. Sola[85a,85b], A. Solano[85a,85b], C. Tarricone[85a,85b], D. Trocino[85a], G. Umoret[85a,85b], R. White[85a,85b], J. Babbar[86a,86b], S. Belforte[86a], V. Candelise[86a,86b], M. Casarsa[86a], F. Cossutti[86a], K. De Leo[86a], G. Della Ricca[86a,86b], R. Delli Gatti[86a,86b], S. Dogra[87], J. Hong[87], J. Kim[87], D. Lee[87], H. Lee[87], J. Lee[87], S.W. Lee[87], C.S. Moon[87], Y.D. Oh[87], M.S. Ryu[87], S. Sekmen[87], B. Tae[87], Y.C. Yang[87], M.S. Kim[88], G. Bak[89], P. Gwak[89], H. Kim[89], D.H. Moon[89], E. Asilar[90], J. Choi[90,be], D. Kim[90], T.J. Kim[90], J.A. Merlin[90], Y. Ryou[90], S. Choi[91], S. Han[91], B. Hong[91], K. Lee[91], K.S. Lee[91], S. Lee[91], J. Yoo[91], J. Goh[92], S. Yang[92], Y. Kang[93], H. S. Kim[93], Y. Kim[93], S. Lee[93], J. Almond[94], J.H. Bhyun[94], J. Choi[94], J. Choi[94], W. Jun[94], J. Kim[94], Y.W. Kim[94], S. Ko[94], H. Lee[94], J. Lee[94], J. Lee[94], B.H. Oh[94], S.B. Oh[94], H. Seo[94], U.K. Yang[94], I. Yoon[94], W. Jang[95], D.Y. Kang[95], S. Kim[95], B. Ko[95], J.S.H. Lee[95], Y. Lee[95], I.C. Park[95], Y. Roh[95], I.J. Watson[95], G. Cho[96], S. Ha[96], K. Hwang[96], B. Kim[96], K. Lee[96], H.D. Yoo[96], M. Choi[97], M.R. Kim[97], H. Lee[97], Y. Lee[97], I. Yu[97], T. Beyrouthy[98], Y. Gharbia[98], F. Alazemi[99], K. Dreimanis[100], A. Gaile[100], C. Munoz Diaz[100], D. Osite[100], G. Pikurs[100], A. Potrebko[100], M. Seidel[100], D. Sidiropoulos Kontos[100], N.R. Strautnieks[101], M. Ambrozas[102], A. Juodagalvis[102], A. Rinkevicius[102], G. Tamulaitis[102], I. Yusuff[103,bf], Z. Zolkapli[103], J.F. Benitez[104], A. Castaneda Hernandez[104], H.A. Encinas Acosta[104], L.G. Gallegos Maríñez[104], M. León Coello[104], J.A. Murillo Quijada[104], A. Sehrawat[104], L. Valencia Palomo[104], G. Ayala[105], H. Castilla-Valdez[105], H. Crotte Ledesma[105], E. De La Cruz-Burelo[105], I. Heredia-De La Cruz[105,bg], R. Lopez-Fernandez[105], J. Mejia Guisao[105], A. Sánchez Hernández[105], C. Oropeza Barrera[106], D.L. Ramirez Guadarrama[106], M. Ramírez García[106], I. Bautista[107], F.E. Neri Huerta[107], I. Pedraza[107], H.A. Salazar Ibarguen[107], C. Uribe Estrada[107],

JHEP06(2026)014

I. Bubanja[108], N. Raicevic[108], P.H. Butler[109], A. Ahmad[110], M.I. Asghar[110], A. Awais[110], M.I.M. Awan[110], H.R. Hoorani[110], W.A. Khan[110], V. Avati[111], A. Bellora[111,bh], L. Forthomme[111], L. Grzanka[111], M. Malawski[111], K. Piotrzkowski[111], H. Bialkowska[112], M. Bluj[112], M. Górski[112], M. Kazana[112], M. Szleper[112], P. Zalewski[112], K. Bunkowski[113], K. Doroba[113], A. Kalinowski[113], M. Konecki[113], J. Krolikowski[113], A. Muhammad[113], P. Fokow[114], K. Pozniak[114], W. Zabolotny[114], M. Araujo[115], D. Bastos[115], C. Beirão Da Cruz E Silva[115], A. Boletti[115], M. Bozzo[115], T. Camporesi[115], G. Da Molin[115], P. Faccioli[115], M. Gallinaro[115], J. Hollar[115], N. Leonardo[115], G.B. Marozzo[115], A. Petrilli[115], M. Pisano[115], J. Seixas[115], J. Varela[115], J.W. Wulff[115], P. Adzic[116], P. Milenovic[116], D. Devetak[117], M. Dordevic[117], J. Milosevic[117], L. Nadderd[117], V. Rekovic[117], M. Stojanovic[117], J. Alcaraz Maestre[118], J.A. Brochero Cifuentes[118], M. Cepeda[118], M. Cerrada[118], N. Colino[118], B. De La Cruz[118], A. Delgado Peris[118], A. Escalante Del Valle[118], Cristina F. Bedoya[118], D. Fernández Del Val[118], J.P. Fernández Ramos[118], J. Flix[118], M.C. Fouz[118], O. Gonzalez Lopez[118], S. Goy Lopez[118], J.M. Hernandez[118], M.I. Josa[118], J. Llorente Merino[118], Oliver M. Carretero[118], C. Martin Perez[118], E. Martin Viscasillas[118], D. Moran[118], C. M. Morcillo Perez[118], Á. Navarro Tobar[118], C. Perez Dengra[118], J. Puerta Pelayo[118], A. Pérez-Calero Yzquierdo[118], I. Redondo[118], J. Sastre[118], J. Vazquez Escobar[118], J.F. de Trocóniz[119], B. Alvarez Gonzalez[120], A. Cardini[120], J. Cuevas[120], J. Del Riego Badas[120], J. Fernandez Menendez[120], S. Folgueras[120], I. Gonzalez Caballero[120], P. Leguina[120], E. Palencia Cortezon[120], J. Prado Pico[120], V. Rodríguez Bouza[120], A. Soto Rodríguez[120], A. Trapote[120], C. Vico Villalba[120], P. Vischia[120], S. Blanco Fernández[121], I.J. Cabrillo[121], A. Calderon[121], J. Duarte Campderros[121], M. Fernandez[121], G. Gomez[121], C. Lasaosa García[121], R. Lopez Ruiz[121], C. Martinez Rivero[121], P. Martinez Ruiz del Arbol[121], F. Matorras[121], P. Matorras Cuevas[121], E. Navarrete Ramos[121], J. Piedra Gomez[121], L. Scodellaro[121], I. Vila[121], J.M. Vizan Garcia[121], D.D.C. Wickramarathna[122], B. Kailasapathy[122,bi], W.G.D. Dharmaratna[123,bj], K. Liyanage[123], N. Perera[123], D. Abbaneo[124], C. Amendola[124], E. Auffray[124], J. Baechler[124], D. Barney[124], A. Bermúdez Martínez[124], M. Bianco[124], A.A. Bin Anuar[124], A. Bocci[124], L. Borgonovi[124], C. Botta[124], A. Bragagnolo[124], E. Brondolin[124], C.E. Brown[124], C. Caillol[124], G. Cerminara[124], N. Chernyavskaya[124], D. d'Enterria[124], A. Dabrowski[124], A. David[124], A. De Roeck[124], M.M. Defranchis[124], M. Deile[124], M. Dobson[124], W. Funk[124], S. Giani[124], D. Gigi[124], K. Gill[124], F. Glege[124], M. Glowacki[124], J. Hegeman[124], J.K. Heikkilä[124], B. Huber[124], V. Innocente[124], T. James[124], P. Janot[124], O. Kaluzinska[124], O. Karacheban[124,aa], G. Karathanasis[124], S. Laurila[124], P. Lecoq[124], E. Leutgeb[124], C. Lourenço[124], M. Magherini[124], L. Malgeri[124], M. Mannelli[124], M. Matthewman[124], A. Mehta[124], F. Meijers[124], S. Mersi[124], E. Meschi[124], M. Migliorini[124], V. Milosevic[124], F. Monti[124], F. Moortgat[124], M. Mulders[124], I. Neutelings[124], S. Orfanelli[124], F. Pantaleo[124], G. Petrucciani[124], A. Pfeiffer[124], M. Pierini[124], M. Pitt[124], H. Qu[124], D. Rabady[124], B. Ribeiro Lopes[124], F. Riti[124], M. Rovere[124], H. Sakulin[124], R. Salvatico[124], S. Sanchez Cruz[124], S. Scarfi[124], M. Selvaggi[124], A. Sharma[124], K. Shchelina[124], P. Silva[124], P. Sphicas[124,bk], A.G. Stahl Leiton[124], A. Steen[124], S. Summers[124],

JHEP06(2026)014

D. Treille[124], P. Tropea[124], D. Walter[124], J. Wanczyk[124,bl], J. Wang[124], S. Wuchterl[124], P. Zehetner[124], P. Zejdl[124], W.D. Zeuner[124], T. Bevilacqua[125,bm], L. Caminada[125,bm], A. Ebrahimi[125], W. Erdmann[125], R. Horisberger[125], Q. Ingram[125], H.C. Kaestli[125], D. Kotlinski[125], C. Lange[125], M. Missiroli[125,bm], L. Noehte[125,bm], T. Rohe[125], A. Samalan[125], T.K. Aarrestad[126], M. Backhaus[126], G. Bonomelli[126], A. Calandri[126], C. Cazzaniga[126], K. Datta[126], P. De Bryas Dexmiers D'archiac[126,bl], A. De Cosa[126], G. Dissertori[126], M. Dittmar[126], M. Donegà[126], F. Eble[126], M. Galli[126], K. Gedia[126], F. Glessgen[126], C. Grab[126], T.G. Harte[126], D. Hits[126], N. Härringer[126], W. Lustermann[126], A.-M. Lyon[126], R.A. Manzoni[126], M. Marchegiani[126], L. Marchese[126], A. Mascellani[126,bl], F. Nessi-Tedaldi[126], F. Pauss[126], V. Perovic[126], S. Pigazzini[126], B. Ristic[126], R. Seidita[126], J. Steggemann[126,bl], A. Tarabini[126], D. Valsecchi[126], R. Wallny[126], C. Amsler[127,bn], P. Bärtschi[127], M.F. Canelli[127], G. Celotto[127], K. Cormier[127], M. Huwiler[127], W. Jin[127], A. Jofrehei[127], B. Kilminster[127], S. Leontsinis[127], S.P. Liechti[127], A. Macchiolo[127], P. Meiring[127], F. Meng[127], J. Motta[127], A. Reimers[127], P. Robmann[127], M. Senger[127], E. Shokr[127], F. Stäger[127], R. Tramontano[127], C. Adloff[128,bo], D. Bhowmik[128], C.M. Kuo[128], W. Lin[128], P.K. Rout[128], P.C. Tiwari[128,al], L. Ceard[129], K.F. Chen[129], Z.g. Chen[129], A. De Iorio[129], W.-S. Hou[129], T.h. Hsu[129], Y.w. Kao[129], S. Karmakar[129], G. Kole[129], Y.y. Li[129], R.-S. Lu[129], E. Paganis[129], X.f. Su[129], J. Thomas-Wilsker[129], L.s. Tsai[129], D. Tsionou[129], H.y. Wu[129], E. Yazgan[129], C. Asawatangtrakuldee[130], N. Srimanobhas[130], V. Wachirapusitanand[130], Y. Maghrbi[131], D. Agyel[132], F. Boran[132], F. Dolek[132], I. Dumanoglu[132,bp], E. Eskut[132], Y. Guler[132,bq], E. Gurpinar Guler[132,bq], C. Isik[132], O. Kara[132], A. Kayis Topaksu[132], Y. Komurcu[132], G. Onengut[132], K. Ozdemir[132,br], A. Polatoz[132], B. Tali[132,bs], U.G. Tok[132], E. Uslan[132], I.S. Zorbakir[132], M. Yalvac[133,bt], B. Akgun[134], I.O. Atakisi[134], E. Gülmez[134], M. Kaya[134,bu], O. Kaya[134,bv], S. Tekten[134,bw], A. Cakir[135], K. Cankocak[135,bp,bx], S. Sen[135,by], O. Aydilek[136,bz], B. Hacisahinoglu[136], I. Hos[136,ca], B. Kaynak[136], S. Ozkorucuklu[136], O. Potok[136], H. Sert[136], C. Simsek[136], C. Zorbilmez[136], S. Cerci[137], B. Isildak[137,cb], D. Sunar Cerci[137], T. Yetkin[137], A. Boyaryntsev[138], B. Grynyov[138], L. Levchuk[139], D. Anthony[140], J.J. Brooke[140], A. Bundock[140], F. Bury[140], E. Clement[140], D. Cussans[140], H. Flacher[140], J. Goldstein[140], H.F. Heath[140], M.-L. Holmberg[140], L. Kreczko[140], S. Paramesvaran[140], L. Robertshaw[140], J. Segal[140], V.J. Smith[140], K. Walkingshaw Pass[140], A.H. Ball[141], K.W. Bell[141], A. Belyaev[141,cc], C. Brew[141], R.M. Brown[141], D.J.A. Cockerill[141], C. Cooke[141], A. Elliot[141], K.V. Ellis[141], K. Harder[141], S. Harper[141], J. Linacre[141], K. Manolopoulos[141], M. Moallemi[141], D.M. Newbold[141], E. Olaiya[141], D. Petyt[141], T. Reis[141], A.R. Sahasransu[141], G. Salvi[141], T. Schuh[141], C.H. Shepherd-Themistocleous[141], I.R. Tomalin[141], K.C. Whalen[141], T. Williams[141], I. Andreou[142], R. Bainbridge[142], P. Bloch[142], O. Buchmuller[142], C.A. Carrillo Montoya[142], G.S. Chahal[142,cd], D. Colling[142], J.S. Dancu[142], I. Das[142], P. Dauncey[142], G. Davies[142], M. Della Negra[142], S. Fayer[142], G. Fedi[142], G. Hall[142], A. Howard[142], G. Iles[142], C.R. Knight[142], P. Krueper[142], J. Langford[142], K.H. Law[142], J. León Holgado[142], L. Lyons[142], A.-M. Magnan[142], B. Maier[142], S. Mallios[142], M. Mieskolainen[142], J. Nash[142,ce], M. Pesaresi[142], P.B. Pradeep[142], B.C. Radburn-Smith[142], A. Richards[142], A. Rose[142], L. Russell[142],

JHEP06(2026)014

K. Savva[142], C. Seez[142], R. Shukla[142], A. Tapper[142], K. Uchida[142], G.P. Uttley[142], T. Virdee[142,ad], M. Vojinovic[142], N. Wardle[142], D. Winterbottom[142], J.E. Cole[143], A. Khan[143], P. Kyberd[143], I.D. Reid[143], S. Abdullin[144], A. Brinkerhoff[144], E. Collins[144], M.R. Darwish[144], J. Dittmann[144], K. Hatakeyama[144], V. Hegde[144], J. Hiltbrand[144], B. McMaster[144], J. Samudio[144], S. Sawant[144], C. Sutantawibul[144], J. Wilson[144], R. Bartek[145], A. Dominguez[145], S. Raj[145], A.E. Simsek[145], S.S. Yu[145], B. Bam[146], A. Buchot Perraguin[146], R. Chudasama[146], S.I. Cooper[146], C. Crovella[146], G. Fidalgo[146], S.V. Gleyzer[146], E. Pearson[146], C.U. Perez[146], P. Rumerio[146,cf], E. Usai[146], R. Yi[146], G. De Castro[147], Z. Demiragli[147], C. Erice[147], C. Fangmeier[147], C. Fernandez Madrazo[147], E. Fontanesi[147], D. Gastler[147], F. Golf[147], S. Jeon[147], J. O'cain[147], I. Reed[147], J. Rohlf[147], K. Salyer[147], D. Sperka[147], D. Spitzbart[147], I. Suarez[147], A. Tsatsos[147], A.G. Zecchinelli[147], G. Barone[148], G. Benelli[148], D. Cutts[148], S. Ellis[148], L. Gouskos[148], M. Hadley[148], U. Heintz[148], K.W. Ho[148], J.M. Hogan[148,cg], T. Kwon[148], G. Landsberg[148], K.T. Lau[148], J. Luo[148], S. Mondal[148], T. Russell[148], S. Sagir[148,ch], X. Shen[148], M. Stamenkovic[148], N. Venkatasubramanian[148], S. Abbott[149], B. Barton[149], C. Brainerd[149], R. Breedon[149], H. Cai[149], M. Calderon De La Barca Sanchez[149], M. Chertok[149], M. Citron[149], J. Conway[149], P.T. Cox[149], R. Erbacher[149], F. Jensen[149], O. Kukral[149], G. Mocellin[149], M. Mulhearn[149], S. Ostrom[149], W. Wei[149], S. Yoo[149], K. Adamidis[150], M. Bachtis[150], D. Campos[150], R. Cousins[150], A. Datta[150], G. Flores Avila[150], J. Hauser[150], M. Ignatenko[150], M.A. Iqbal[150], T. Lam[150], Y.f. Lo[150], E. Manca[150], A. Nunez Del Prado[150], D. Saltzberg[150], V. Valuev[150], R. Clare[151], J.W. Gary[151], G. Hanson[151], A. Aportela[152], A. Arora[152], J.G. Branson[152], S. Cittolin[152], S. Cooperstein[152], D. Diaz[152], J. Duarte[152], L. Giannini[152], Y. Gu[152], J. Guiang[152], R. Kansal[152], V. Krutelyov[152], R. Lee[152], J. Letts[152], M. Masciovecchio[152], F. Mokhtar[152], S. Mukherjee[152], M. Pieri[152], D. Primosch[152], M. Quinnan[152], V. Sharma[152], M. Tadel[152], E. Vourliotis[152], F. Würthwein[152], Y. Xiang[152], A. Yagil[152], A. Barzdukas[153], L. Brennan[153], C. Campagnari[153], K. Downham[153], C. Grieco[153], M.M. Hussain[153], J. Incandela[153], J. Kim[153], A.J. Li[153], P. Masterson[153], H. Mei[153], J. Richman[153], S.N. Santpur[153], U. Sarica[153], R. Schmitz[153], F. Setti[153], J. Sheplock[153], D. Stuart[153], T.Á. Vámi[153], X. Yan[153], D. Zhang[153], A. Albert[154], S. Bhattacharya[154], A. Bornheim[154], O. Cerri[154], J. Mao[154], H.B. Newman[154], G. Reales Gutiérrez[154], M. Spiropulu[154], J.R. Vlimant[154], S. Xie[154], R.Y. Zhu[154], J. Alison[155], S. An[155], P. Bryant[155], M. Cremonesi[155], V. Dutta[155], T. Ferguson[155], T.A. Gómez Espinosa[155], A. Harilal[155], A. Kallil Tharayil[155], M. Kanemura[155], C. Liu[155], T. Mudholkar[155], S. Murthy[155], P. Palit[155], K. Park[155], M. Paulini[155], A. Roberts[155], A. Sanchez[155], W. Terrill[155], J.P. Cumalat[156], W.T. Ford[156], A. Hart[156], A. Hassani[156], N. Manganelli[156], J. Pearkes[156], C. Savard[156], N. Schonbeck[156], K. Stenson[156], K.A. Ulmer[156], S.R. Wagner[156], N. Zipper[156], D. Zuolo[156], J. Alexander[157], X. Chen[157], D.J. Cranshaw[157], J. Dickinson[157], J. Fan[157], X. Fan[157], J. Grassi[157], S. Hogan[157], P. Kotamnives[157], J. Monroy[157], G. Niendorf[157], M. Oshiro[157], J.R. Patterson[157], M. Reid[157], A. Ryd[157], J. Thom[157], P. Wittich[157], R. Zou[157], M. Albrow[158], M. Alyari[158], O. Amram[158], G. Apollinari[158], A. Apresyan[158], L.A.T. Bauerdick[158], D. Berry[158], J. Berryhill[158], P.C. Bhat[158], K. Burkett[158],

JHEP06(2026)014

J.N. Butler[158], A. Canepa[158], G.B. Cerati[158], H.W.K. Cheung[158], F. Chlebana[158], C. Cosby[158], G. Cummings[158], I. Dutta[158], V.D. Elvira[158], J. Freeman[158], A. Gandrakota[158], Z. Gecse[158], L. Gray[158], D. Green[158], A. Grummer[158], S. Grünendahl[158], D. Guerrero[158], O. Gutsche[158], R.M. Harris[158], T.C. Herwig[158], J. Hirschauer[158], B. Jayatilaka[158], S. Jindariani[158], M. Johnson[158], U. Joshi[158], T. Klijnsma[158], B. Klima[158], K.H.M. Kwok[158], S. Lammel[158], C. Lee[158], D. Lincoln[158], R. Lipton[158], T. Liu[158], K. Maeshima[158], D. Mason[158], P. McBride[158], P. Merkel[158], S. Mrenna[158], S. Nahn[158], J. Ngadiuba[158], D. Noonan[158], S. Norberg[158], V. Papadimitriou[158], N. Pastika[158], K. Pedro[158], C. Pena[158,ci], F. Ravera[158], A. Reinsvold Hall[158,cj], L. Ristori[158], M. Safdari[158], E. Sexton-Kennedy[158], N. Smith[158], A. Soha[158], L. Spiegel[158], S. Stoynev[158], J. Strait[158], L. Taylor[158], S. Tkaczyk[158], N.V. Tran[158], L. Uplegger[158], E.W. Vaandering[158], C. Wang[158], I. Zoi[158], C. Aruta[159], P. Avery[159], D. Bourilkov[159], P. Chang[159], V. Cherepanov[159], R.D. Field[159], C. Huh[159], E. Koenig[159], M. Kolosova[159], J. Konigsberg[159], A. Korytov[159], K. Matchev[159], N. Menendez[159], G. Mitselmakher[159], K. Mohrman[159], A. Muthirakalayil Madhu[159], N. Rawal[159], S. Rosenzweig[159], Y. Takahashi[159], J. Wang[159], T. Adams[160], A. Al Kadhim[160], A. Askew[160], S. Bower[160], R. Hashmi[160], R.S. Kim[160], S. Kim[160], T. Kolberg[160], G. Martinez[160], H. Prosper[160], P.R. Prova[160], M. Wulansatiti[160], R. Yohay[160], J. Zhang[160], B. Alsufyani[161], S. Butalla[161], S. Das[161], T. Elkafrawy[161,ck], M. Hohlmann[161], M. Lavinsky[161], E. Yanes[161], M.R. Adams[162], A. Baty[162], C. Bennett[162], R. Cavanaugh[162], D. S. Lemos[162], R. Escobar Franco[162], O. Evdokimov[162], C.E. Gerber[162], H. Gupta[162], M. Hawksworth[162], A. Hingrajiya[162], D.J. Hofman[162], J.h. Lee[162], C. Mills[162], S. Nanda[162], B. Ozek[162], T. Phan[162], D. Pilipovic[162], R. Pradhan[162], E. Prifti[162], P. Roy[162], T. Roy[162], S. Rudrabhatla[162], N. Singh[162], M.B. Tonjes[162], N. Varelas[162], M.A. Wadud[162], Z. Ye[162], J. Yoo[162], M. Alhusseini[163], D. Blend[163], K. Dilsiz[163,cl], L. Emediato[163], G. Karaman[163], O.K. Köseyan[163], J.-P. Merlo[163], A. Mestvirishvili[163,cm], O. Neogi[163], H. Ogul[163,cn], Y. Onel[163], A. Penzo[163], C. Snyder[163], E. Tiras[163,co], B. Blumenfeld[164], L. Corcodilos[164], J. Davis[164], A.V. Gritsan[164], L. Kang[164], S. Kyriacou[164], P. Maksimovic[164], M. Roguljic[164], J. Roskes[164], S. Sekhar[164], M. Swartz[164], A. Abreu[165], L.F. Alcerro Alcerro[165], J. Anguiano[165], S. Arteaga Escatel[165], P. Baringer[165], A. Bean[165], Z. Flowers[165], D. Grove[165], J. King[165], G. Krintiras[165], M. Lazarovits[165], C. Le Mahieu[165], J. Marquez[165], M. Murray[165], M. Nickel[165], S. Popescu[165,cp], C. Rogan[165], C. Royon[165], S. Sanders[165], C. Smith[165], G. Wilson[165], B. Allmond[166], A. Ivanov[166], K. Kaadze[166], Y. Maravin[166], J. Natoli[166], R. Gujju Gurunadha[166], D. Roy[166], G. Sorrentino[166], A. Baden[167], A. Belloni[167], J. Bistany-riebman[167], S.C. Eno[167], N.J. Hadley[167], S. Jabeen[167], R.G. Kellogg[167], T. Koeth[167], B. Kronheim[167], S. Lascio[167], P. Major[167], A.C. Mignerey[167], S. Nabili[167], C. Palmer[167], C. Papageorgakis[167], M.M. Paranjpe[167], E. Popova[167,cq], A. Shevelev[167], L. Wang[167], L. Zhang[167], C. Baldenegro Barrera[168], J. Bendavid[168], S. Bright-Thonney[168], I.A. Cali[168], P.c. Chou[168], M. D'Alfonso[168], J. Eysermans[168], C. Freer[168], G. Gomez-Ceballos[168], M. Goncharov[168], G. Grosso[168], P. Harris[168], D. Hoang[168], D. Kovalskyi[168], J. Krupa[168], L. Lavezzo[168], Y.-J. Lee[168], K. Long[168], C. Mcginn[168], A. Novak[168], M.I. Park[168], C. Paus[168], C. Reissel[168],

JHEP06(2026)014

C. Roland[168], G. Roland[168], S. Rothman[168], G.S.F. Stephans[168], Z. Wang[168], B. Wyslouch[168], T. J. Yang[168], B. Crossman[169], C. Kapsiak[169], M. Krohn[169], D. Mahon[169], J. Mans[169], B. Marzocchi[169], M. Revering[169], R. Rusack[169], R. Saradhy[169], N. Strobbe[169], K. Bloom[170], D.R. Claes[170], G. Haza[170], J. Hossain[170], C. Joo[170], I. Kravchenko[170], A. Rohilla[170], J.E. Siado[170], W. Tabb[170], A. Vagnerini[170], A. Wightman[170], F. Yan[170], D. Yu[170], H. Bandyopadhyay[171], L. Hay[171], H.w. Hsia[171], I. Iashvili[171], A. Kalogeropoulos[171], A. Kharchilava[171], A. Mandal[171], M. Morris[171], D. Nguyen[171], S. Rappoccio[171], H. Rejeb Sfar[171], A. Williams[171], P. Young[171], G. Alverson[172], E. Barberis[172], J. Bonilla[172], B. Bylsma[172], M. Campana[172], J. Dervan[172], Y. Haddad[172], Y. Han[172], I. Israr[172], A. Krishna[172], P. Levchenko[172], J. Li[172], M. Lu[172], R. Mccarthy[172], D.M. Morse[172], T. Orimoto[172], A. Parker[172], L. Skinnari[172], C.S. Thoreson[172], E. Tsai[172], D. Wood[172], S. Dittmer[173], K.A. Hahn[173], D. Li[173], Y. Liu[173], M. Mcginnis[173], Y. Miao[173], D.G. Monk[173], M.H. Schmitt[173], A. Taliercio[173], M. Velasco[173], G. Agarwal[174], R. Band[174], R. Bucci[174], S. Castells[174], A. Das[174], R. Goldouzian[174], M. Hildreth[174], K. Hurtado Anampa[174], T. Ivanov[174], C. Jessop[174], K. Lannon[174], J. Lawrence[174], N. Loukas[174], L. Lutton[174], J. Mariano[174], N. Marinelli[174], I. Mcalister[174], T. McCauley[174], C. Mcgrady[174], C. Moore[174], Y. Musienko[174,cr], H. Nelson[174], M. Osherson[174], A. Piccinelli[174], R. Ruchti[174], A. Townsend[174], Y. Wan[174], M. Wayne[174], H. Yockey[174], M. Zarucki[174], L. Zygala[174], A. Basnet[175], M. Carrigan[175], L.S. Durkin[175], C. Hill[175], M. Joyce[175], M. Nunez Ornelas[175], K. Wei[175], D.A. Wenzl[175], B.L. Winer[175], B. R. Yates[175], H. Bouchamaoui[176], K. Coldham[176], P. Das[176], G. Dezoort[176], P. Elmer[176], P. Fackeldey[176], A. Frankenthal[176], B. Greenberg[176], N. Haubrich[176], K. Kennedy[176], G. Kopp[176], S. Kwan[176], Y. Lai[176], D. Lange[176], A. Loeliger[176], D. Marlow[176], I. Ojalvo[176], J. Olsen[176], F. Simpson[176], D. Stickland[176], C. Tully[176], L.H. Vage[176], S. Malik[177], R. Sharma[177], A.S. Bakshi[178], S. Chandra[178], R. Chawla[178], A. Gu[178], L. Gutay[178], M. Jones[178], A.W. Jung[178], A. K. Virdi[178], M. Liu[178], G. Negro[178], N. Neumeister[178], G. Paspalaki[178], S. Piperov[178], J.F. Schulte[178], F. Wang[178], A. Wildridge[178], W. Xie[178], Y. Yao[178], J. Dolen[179], N. Parashar[179], A. Pathak[179], D. Acosta[180], A. Agrawal[180], T. Carnahan[180], K.M. Ecklund[180], P.J. Fernández Manteca[180], S. Freed[180], P. Gardner[180], F.J.M. Geurts[180], T. Huang[180], I. Krommydas[180], W. Li[180], J. Lin[180], O. Miguel Colin[180], B.P. Padley[180], R. Redjimi[180], J. Rotter[180], E. Yigitbasi[180], Y. Zhang[180], A. Bodek[181], P. de Barbaro[181], R. Demina[181], J.L. Dulemba[181], A. Garcia-Bellido[181], O. Hindrichs[181], A. Khukhunaishvili[181], N. Parmar[181], P. Parygin[181,cq], R. Taus[181], B. Chiarito[182], J.P. Chou[182], S.V. Clark[182], D. Gadkari[182], Y. Gershtein[182], E. Halkiadakis[182], C. Houghton[182], D. Jaroslawski[182], S. Konstantinou[182], I. Laflotte[182], A. Lath[182], J. Martins[182], R. Montalvo[182], K. Nash[182], M. Heindl[182], J. Reichert[182], P. Saha[182], S. Salur[182], S. Schnetzer[182], S. Somalwar[182], R. Stone[182], S.A. Thayil[182], S. Thomas[182], J. Vora[182], D. Ally[183], A.G. Delannoy[183], S. Fiorendi[183], S. Higginbotham[183], T. Holmes[183], A.R. Kanuganti[183], N. Karunarathna[183], L. Lee[183], E. Nibigira[183], S. Spanier[183], D. Aebi[184], M. Ahmad[184], T. Akhter[184], K. Androsov[184], A. Bolshov[184], O. Bouhali[184,cs], R. Eusebi[184], J. Gilmore[184], T. Kamon[184], H. Kim[184], S. Luo[184], R. Mueller[184], A. Safonov[184], N. Akchurin[185], J. Damgov[185], Y. Feng[185], N. Gogate[185],

JHEP06(2026)014

Y. Kazhykarim[185], K. Lamichhane[185], S.W. Lee[185], C. Madrid[185], A. Mankel[185], T. Peltola[185], I. Volobouev[185], E. Appelt[186], Y. Chen[186], S. Greene[186], A. Gurrola[186], W. Johns[186], R. Kunnawalkam Elayavalli[186], A. Melo[186], D. Rathjens[186], F. Romeo[186], P. Sheldon[186], S. Tuo[186], J. Velkovska[186], J. Viinikainen[186], B. Cardwell[187], H. Chung[187], B. Cox[187], J. Hakala[187], R. Hirosky[187], A. Ledovskoy[187], C. Mantilla[187], C. Neu[187], C. Ramón Álvarez[187], S. Bhattacharya[188], P.E. Karchin[188], A. Aravind[189], S. Banerjee[189], K. Black[189], T. Bose[189], E. Chavez[189], S. Dasu[189], P. Everaerts[189], C. Galloni[189], H. He[189], M. Herndon[189], A. Herve[189], C.K. Koraka[189], A. Lanaro[189], S. Lomte[189], R. Loveless[189], A. Mallampalli[189], A. Mohammadi[189], S. Mondal[189], G. Parida[189], D. Pinna[189], L. Pétré[189], A. Savin[189], V. Shang[189], V. Sharma[189], W.H. Smith[189], D. Teague[189], H.F. Tsoi[189], W. Vetens[189], A. Warden[189], S. Afanasiev[190], V. Alexakhin[190], Yu. Andreev[190], T. Aushev[190], D. Budkouski[190], M. Danilov[190,cr], T. Dimova[190,cr], A. Ershov[190,cr], I. Golutvin[190,†], I. Gorbunov[190], A. Gribushin[190,cr], V. Karjavine[190], M. Kirsanov[190], V. Klyukhin[190,cr], O. Kodolova[190,ct,cq], V. Korenkov[190], A. Kozyrev[190,cr], A. Lanev[190], A. Malakhov[190], V. Matveev[190,cr], A. Nikitenko[190,cu,cv], V. Palichik[190], V. Perelygin[190], S. Petrushanko[190,cr], S. Polikarpov[190,cr], O. Radchenko[190,cr], M. Savina[190], V. Shalaev[190], S. Shmatov[190], S. Shulha[190], Y. Skovpen[190,cr], V. Smirnov[190], O. Teryaev[190], I. Tlisova[190,cr], A. Toropin[190], N. Voytishin[190], B.S. Yuldashev[190,cw,†], A. Zarubin[190], I. Zhizhin[190], V. Andreev[191], M. Azarkin[191], A. Babaev[191], V. Blinov[191,cr], E. Boos[191], V. Borshch[191], V. Bunichev[191], R. Chistov[191,cr], A. Dermenev[191], D. Druzhkin[191], M. Dubinin[191,ci], L. Dudko[191], G. Gavrilov[191], V. Gavrilov[191], S. Gninenko[191], V. Golovtcov[191], N. Golubev[191], Y. Ivanov[191], K. Ivanov[191], V. Kachanov[191], A. Karneyeu[191], V. Kim[191,cr], M. Kirakosyan[191], D. Kirpichnikov[191], N. Krasnikov[191], N. Lychkovskaya[191], V. Murzin[191], V. Oreshkin[191], M. Perfilov[191], V. Popov[191], V. Savrin[191], S. Slabospitskii[191], D. Sosnov[191], V. Sulimov[191], A. Terkulov[191], L. Uvarov[191], A. Uzunian[191], A. Vorobyev[191,†], A. Zhokin[191]

[1] *Yerevan Physics Institute, Yerevan, Armenia*
[2] *Institut für Hochenergiephysik, Vienna, Austria*
[3] *Universiteit Antwerpen, Antwerpen, Belgium*
[4] *Vrije Universiteit Brussel, Brussel, Belgium*
[5] *Université Libre de Bruxelles, Bruxelles, Belgium*
[6] *Ghent University, Ghent, Belgium*
[7] *Université Catholique de Louvain, Louvain-la-Neuve, Belgium*
[8] *Centro Brasileiro de Pesquisas Fisicas, Rio de Janeiro, Brazil*
[9] *Universidade do Estado do Rio de Janeiro, Rio de Janeiro, Brazil*
[10] *Universidade Estadual Paulista, Universidade Federal do ABC, São Paulo, Brazil*
[11] *Institute for Nuclear Research and Nuclear Energy, Bulgarian Academy of Sciences, Sofia, Bulgaria*
[12] *University of Sofia, Sofia, Bulgaria*
[13] *Instituto De Alta Investigación, Universidad de Tarapacá, Casilla 7 D, Arica, Chile*
[14] *Beihang University, Beijing, China*
[15] *Department of Physics, Tsinghua University, Beijing, China*
[16] *Institute of High Energy Physics, Beijing, China*
[17] *State Key Laboratory of Nuclear Physics and Technology, Peking University, Beijing, China*
[18] *State Key Laboratory of Nuclear Physics and Technology, Institute of Quantum Matter, South China Normal University, Guangzhou, China*

JHEP06(2026)014

[19] Sun Yat-Sen University, Guangzhou, China
[20] University of Science and Technology of China, Hefei, China
[21] Nanjing Normal University, Nanjing, China
[22] Institute of Modern Physics and Key Laboratory of Nuclear Physics and Ion-beam Application (MOE) — Fudan University, Shanghai, China
[23] Zhejiang University, Hangzhou, Zhejiang, China
[24] Universidad de Los Andes, Bogota, Colombia
[25] Universidad de Antioquia, Medellin, Colombia
[26] University of Split, Faculty of Electrical Engineering, Mechanical Engineering and Naval Architecture, Split, Croatia
[27] University of Split, Faculty of Science, Split, Croatia
[28] Institute Rudjer Boskovic, Zagreb, Croatia
[29] University of Cyprus, Nicosia, Cyprus
[30] Charles University, Prague, Czech Republic
[31] Escuela Politecnica Nacional, Quito, Ecuador
[32] Universidad San Francisco de Quito, Quito, Ecuador
[33] Academy of Scientific Research and Technology of the Arab Republic of Egypt, Egyptian Network of High Energy Physics, Cairo, Egypt
[34] Center for High Energy Physics (CHEP-FU), Fayoum University, El-Fayoum, Egypt
[35] National Institute of Chemical Physics and Biophysics, Tallinn, Estonia
[36] Department of Physics, University of Helsinki, Helsinki, Finland
[37] Helsinki Institute of Physics, Helsinki, Finland
[38] Lappeenranta-Lahti University of Technology, Lappeenranta, Finland
[39] IRFU, CEA, Université Paris-Saclay, Gif-sur-Yvette, France
[40] Laboratoire Leprince-Ringuet, CNRS/IN2P3, Ecole Polytechnique, Institut Polytechnique de Paris, Palaiseau, France
[41] Université de Strasbourg, CNRS, IPHC UMR 7178, Strasbourg, France
[42] Centre de Calcul de l'Institut National de Physique Nucleaire et de Physique des Particules, CNRS/IN2P3, Villeurbanne, France
[43] Institut de Physique des 2 Infinis de Lyon (IP2I), Villeurbanne, France
[44] Georgian Technical University, Tbilisi, Georgia
[45] RWTH Aachen University, I. Physikalisches Institut, Aachen, Germany
[46] RWTH Aachen University, III. Physikalisches Institut A, Aachen, Germany
[47] RWTH Aachen University, III. Physikalisches Institut B, Aachen, Germany
[48] Deutsches Elektronen-Synchrotron, Hamburg, Germany
[49] University of Hamburg, Hamburg, Germany
[50] Karlsruher Institut fuer Technologie, Karlsruhe, Germany
[51] Institute of Nuclear and Particle Physics (INPP), NCSR Demokritos, Aghia Paraskevi, Greece
[52] National and Kapodistrian University of Athens, Athens, Greece
[53] National Technical University of Athens, Athens, Greece
[54] University of Ioánnina, Ioánnina, Greece
[55] HUN-REN Wigner Research Centre for Physics, Budapest, Hungary
[56] MTA-ELTE Lendület CMS Particle and Nuclear Physics Group, Eötvös Loránd University, Budapest, Hungary
[57] Faculty of Informatics, University of Debrecen, Debrecen, Hungary
[58] HUN-REN ATOMKI — Institute of Nuclear Research, Debrecen, Hungary
[59] Karoly Robert Campus, MATE Institute of Technology, Gyongyos, Hungary
[60] Panjab University, Chandigarh, India
[61] University of Delhi, Delhi, India
[62] Indian Institute of Technology Kanpur, Kanpur, India
[63] Saha Institute of Nuclear Physics, HBNI, Kolkata, India
[64] Indian Institute of Technology Madras, Madras, India
[65] Tata Institute of Fundamental Research-A, Mumbai, India

JHEP06(2026)014

[66] Tata Institute of Fundamental Research-B, Mumbai, India
[67] National Institute of Science Education and Research, An OCC of Homi Bhabha National Institute, Bhubaneswar, Odisha, India
[68] Indian Institute of Science Education and Research (IISER), Pune, India
[69] Isfahan University of Technology, Isfahan, Iran
[70] Institute for Research in Fundamental Sciences (IPM), Tehran, Iran
[71] University College Dublin, Dublin, Ireland
[72a] INFN Sezione di Bari, Bari, Italy
[72b] Università di Bari, Bari, Italy
[72c] Politecnico di Bari, Bari, Italy
[73a] INFN Sezione di Bologna, Bologna, Italy
[73b] Università di Bologna, Bologna, Italy
[74a] INFN Sezione di Catania, Catania, Italy
[74b] Università di Catania, Catania, Italy
[75a] INFN Sezione di Firenze, Firenze, Italy
[75b] Università di Firenze, Firenze, Italy
[76] INFN Laboratori Nazionali di Frascati, Frascati, Italy
[77a] INFN Sezione di Genova, Genova, Italy
[77b] Università di Genova, Genova, Italy
[78a] INFN Sezione di Milano-Bicocca, Milano, Italy
[78b] Università di Milano-Bicocca, Milano, Italy
[79a] INFN Sezione di Napoli, Napoli, Italy
[79b] Università di Napoli 'Federico II', Napoli, Italy
[79c] Università della Basilicata, Potenza, Italy
[80a] INFN Sezione di Padova, Padova, Italy
[80b] Università di Padova, Padova, Italy
[81a] INFN Sezione di Pavia, Pavia, Italy
[81b] Università di Pavia, Pavia, Italy
[82a] INFN Sezione di Perugia, Perugia, Italy
[82b] Università di Perugia, Perugia, Italy
[83a] INFN Sezione di Pisa, Pisa, Italy
[83b] Università di Pisa, Pisa, Italy
[83c] Scuola Normale Superiore di Pisa, Pisa, Italy
[83d] Università di Siena, Siena, Italy
[84a] INFN Sezione di Roma, Roma, Italy
[84b] Sapienza Università di Roma, Roma, Italy
[85a] INFN Sezione di Torino, Torino, Italy
[85b] Università di Torino, Torino, Italy
[85c] Università del Piemonte Orientale, Novara, Italy
[86a] INFN Sezione di Trieste, Trieste, Italy
[86b] Università di Trieste, Trieste, Italy
[87] Kyungpook National University, Daegu, Korea
[88] Department of Mathematics and Physics — GWNU, Gangneung, Korea
[89] Chonnam National University, Institute for Universe and Elementary Particles, Kwangju, Korea
[90] Hanyang University, Seoul, Korea
[91] Korea University, Seoul, Korea
[92] Kyung Hee University, Department of Physics, Seoul, Korea
[93] Sejong University, Seoul, Korea
[94] Seoul National University, Seoul, Korea
[95] University of Seoul, Seoul, Korea
[96] Yonsei University, Department of Physics, Seoul, Korea
[97] Sungkyunkwan University, Suwon, Korea
[98] College of Engineering and Technology, American University of the Middle East (AUM), Dasman, Kuwait

JHEP06(2026)014

[99] *Kuwait University — College of Science — Department of Physics, Safat, Kuwait*
[100] *Riga Technical University, Riga, Latvia*
[101] *University of Latvia (LU), Riga, Latvia*
[102] *Vilnius University, Vilnius, Lithuania*
[103] *National Centre for Particle Physics, Universiti Malaya, Kuala Lumpur, Malaysia*
[104] *Universidad de Sonora (UNISON), Hermosillo, Mexico*
[105] *Centro de Investigacion y de Estudios Avanzados del IPN, Mexico City, Mexico*
[106] *Universidad Iberoamericana, Mexico City, Mexico*
[107] *Benemerita Universidad Autonoma de Puebla, Puebla, Mexico*
[108] *University of Montenegro, Podgorica, Montenegro*
[109] *University of Canterbury, Christchurch, New Zealand*
[110] *National Centre for Physics, Quaid-I-Azam University, Islamabad, Pakistan*
[111] *AGH University of Krakow, Krakow, Poland*
[112] *National Centre for Nuclear Research, Swierk, Poland*
[113] *Institute of Experimental Physics, Faculty of Physics, University of Warsaw, Warsaw, Poland*
[114] *Warsaw University of Technology, Warsaw, Poland*
[115] *Laboratório de Instrumentação e Física Experimental de Partículas, Lisboa, Portugal*
[116] *Faculty of Physics, University of Belgrade, Belgrade, Serbia*
[117] *VINCA Institute of Nuclear Sciences, University of Belgrade, Belgrade, Serbia*
[118] *Centro de Investigaciones Energéticas Medioambientales y Tecnológicas (CIEMAT), Madrid, Spain*
[119] *Universidad Autónoma de Madrid, Madrid, Spain*
[120] *Universidad de Oviedo, Instituto Universitario de Ciencias y Tecnologías Espaciales de Asturias (ICTEA), Oviedo, Spain*
[121] *Instituto de Física de Cantabria (IFCA), CSIC-Universidad de Cantabria, Santander, Spain*
[122] *University of Colombo, Colombo, Sri Lanka*
[123] *University of Ruhuna, Department of Physics, Matara, Sri Lanka*
[124] *CERN, European Organization for Nuclear Research, Geneva, Switzerland*
[125] *PSI Center for Neutron and Muon Sciences, Villigen, Switzerland*
[126] *ETH Zurich — Institute for Particle Physics and Astrophysics (IPA), Zurich, Switzerland*
[127] *Universität Zürich, Zurich, Switzerland*
[128] *National Central University, Chung-Li, Taiwan*
[129] *National Taiwan University (NTU), Taipei, Taiwan*
[130] *High Energy Physics Research Unit, Department of Physics, Faculty of Science, Chulalongkorn University, Bangkok, Thailand*
[131] *Tunis El Manar University, Tunis, Tunisia*
[132] *Çukurova University, Physics Department, Science and Art Faculty, Adana, Turkey*
[133] *Middle East Technical University, Physics Department, Ankara, Turkey*
[134] *Bogazici University, Istanbul, Turkey*
[135] *Istanbul Technical University, Istanbul, Turkey*
[136] *Istanbul University, Istanbul, Turkey*
[137] *Yildiz Technical University, Istanbul, Turkey*
[138] *Institute for Scintillation Materials of National Academy of Science of Ukraine, Kharkiv, Ukraine*
[139] *National Science Centre, Kharkiv Institute of Physics and Technology, Kharkiv, Ukraine*
[140] *University of Bristol, Bristol, United Kingdom*
[141] *Rutherford Appleton Laboratory, Didcot, United Kingdom*
[142] *Imperial College, London, United Kingdom*
[143] *Brunel University, Uxbridge, United Kingdom*
[144] *Baylor University, Waco, Texas, U.S.A.*
[145] *Catholic University of America, Washington, DC, U.S.A.*
[146] *The University of Alabama, Tuscaloosa, Alabama, U.S.A.*
[147] *Boston University, Boston, Massachusetts, U.S.A.*
[148] *Brown University, Providence, Rhode Island, U.S.A.*
[149] *University of California, Davis, Davis, California, U.S.A.*

JHEP06(2026)014

[150] University of California, Los Angeles, California, U.S.A.
[151] University of California, Riverside, Riverside, California, U.S.A.
[152] University of California, San Diego, La Jolla, California, U.S.A.
[153] University of California, Santa Barbara — Department of Physics, Santa Barbara, California, U.S.A.
[154] California Institute of Technology, Pasadena, California, U.S.A.
[155] Carnegie Mellon University, Pittsburgh, Pennsylvania, U.S.A.
[156] University of Colorado Boulder, Boulder, Colorado, U.S.A.
[157] Cornell University, Ithaca, New York, U.S.A.
[158] Fermi National Accelerator Laboratory, Batavia, Illinois, U.S.A.
[159] University of Florida, Gainesville, Florida, U.S.A.
[160] Florida State University, Tallahassee, Florida, U.S.A.
[161] Florida Institute of Technology, Melbourne, Florida, U.S.A.
[162] University of Illinois Chicago, Chicago, Illinois, U.S.A.
[163] The University of Iowa, Iowa City, Iowa, U.S.A.
[164] Johns Hopkins University, Baltimore, Maryland, U.S.A.
[165] The University of Kansas, Lawrence, Kansas, U.S.A.
[166] Kansas State University, Manhattan, Kansas, U.S.A.
[167] University of Maryland, College Park, Maryland, U.S.A.
[168] Massachusetts Institute of Technology, Cambridge, Massachusetts, U.S.A.
[169] University of Minnesota, Minneapolis, Minnesota, U.S.A.
[170] University of Nebraska-Lincoln, Lincoln, Nebraska, U.S.A.
[171] State University of New York at Buffalo, Buffalo, New York, U.S.A.
[172] Northeastern University, Boston, Massachusetts, U.S.A.
[173] Northwestern University, Evanston, Illinois, U.S.A.
[174] University of Notre Dame, Notre Dame, Indiana, U.S.A.
[175] The Ohio State University, Columbus, Ohio, U.S.A.
[176] Princeton University, Princeton, New Jersey, U.S.A.
[177] University of Puerto Rico, Mayaguez, Puerto Rico, U.S.A.
[178] Purdue University, West Lafayette, Indiana, U.S.A.
[179] Purdue University Northwest, Hammond, Indiana, U.S.A.
[180] Rice University, Houston, Texas, U.S.A.
[181] University of Rochester, Rochester, New York, U.S.A.
[182] Rutgers, The State University of New Jersey, Piscataway, New Jersey, U.S.A.
[183] University of Tennessee, Knoxville, Tennessee, U.S.A.
[184] Texas A&M University, College Station, Texas, U.S.A.
[185] Texas Tech University, Lubbock, Texas, U.S.A.
[186] Vanderbilt University, Nashville, Tennessee, U.S.A.
[187] University of Virginia, Charlottesville, Virginia, U.S.A.
[188] Wayne State University, Detroit, Michigan, U.S.A.
[189] University of Wisconsin — Madison, Madison, Wisconsin, U.S.A.
[190] An institute or international laboratory covered by a cooperation agreement with CERN
[191] An institute formerly covered by a cooperation agreement with CERN

[a] Also at Yerevan State University, Yerevan, Armenia
[b] Also at TU Wien, Vienna, Austria
[c] Also at Ghent University, Ghent, Belgium
[d] Also at Universidade do Estado do Rio de Janeiro, Rio de Janeiro, Brazil
[e] Also at FACAMP — Faculdades de Campinas, Sao Paulo, Brazil
[f] Also at Universidade Estadual de Campinas, Campinas, Brazil
[g] Also at Federal University of Rio Grande do Sul, Porto Alegre, Brazil
[h] Also at University of Chinese Academy of Sciences, Beijing, China
[i] Also at China Center of Advanced Science and Technology, Beijing, China
[j] Also at University of Chinese Academy of Sciences, Beijing, China

JHEP06(2026)014

[k] Also at China Spallation Neutron Source, Guangdong, China
[l] Now at Henan Normal University, Xinxiang, China
[m] Also at University of Shanghai for Science and Technology, Shanghai, China
[n] Now at The University of Iowa, Iowa City, Iowa, U.S.A.
[o] Also at Cairo University, Cairo, Egypt
[p] Also at Helwan University, Cairo, Egypt
[q] Also at Suez University, Suez, Egypt
[r] Now at British University in Egypt, Cairo, Egypt
[s] Also at Purdue University, West Lafayette, Indiana, U.S.A.
[t] Also at Université de Haute Alsace, Mulhouse, France
[u] Also at Istinye University, Istanbul, Turkey
[v] Also at Another institute or international laboratory covered by a cooperation agreement with CERN
[w] Also at The University of the State of Amazonas, Manaus, Brazil
[x] Also at University of Hamburg, Hamburg, Germany
[y] Also at RWTH Aachen University, III. Physikalisches Institut A, Aachen, Germany
[z] Also at Bergische University Wuppertal (BUW), Wuppertal, Germany
[aa] Also at Brandenburg University of Technology, Cottbus, Germany
[ab] Also at Forschungszentrum Jülich, Juelich, Germany
[ac] Now at RWTH Aachen University, III. Physikalisches Institut A, Aachen, Germany
[ad] Also at CERN, European Organization for Nuclear Research, Geneva, Switzerland
[ae] Also at HUN-REN ATOMKI — Institute of Nuclear Research, Debrecen, Hungary
[af] Now at Universitatea Babes-Bolyai — Facultatea de Fizica, Cluj-Napoca, Romania
[ag] Also at MTA-ELTE Lendület CMS Particle and Nuclear Physics Group, Eötvös Loránd University, Budapest, Hungary
[ah] Also at HUN-REN Wigner Research Centre for Physics, Budapest, Hungary
[ai] Also at Physics Department, Faculty of Science, Assiut University, Assiut, Egypt
[aj] Also at Punjab Agricultural University, Ludhiana, India
[ak] Also at University of Visva-Bharati, Santiniketan, India
[al] Also at Indian Institute of Science (IISc), Bangalore, India
[am] Also at Amity University Uttar Pradesh, Noida, India
[an] Also at UPES — University of Petroleum and Energy Studies, Dehradun, India
[ao] Also at IIT Bhubaneswar, Bhubaneswar, India
[ap] Also at Institute of Physics, Bhubaneswar, India
[aq] Also at University of Hyderabad, Hyderabad, India
[ar] Also at Deutsches Elektronen-Synchrotron, Hamburg, Germany
[as] Also at Isfahan University of Technology, Isfahan, Iran
[at] Also at Sharif University of Technology, Tehran, Iran
[au] Also at Department of Physics, University of Science and Technology of Mazandaran, Behshahr, Iran
[av] Also at Department of Physics, Faculty of Science, Arak University, ARAK, Iran
[aw] Also at Italian National Agency for New Technologies, Energy and Sustainable Economic Development, Bologna, Italy
[ax] Also at Centro Siciliano di Fisica Nucleare e di Struttura Della Materia, Catania, Italy
[ay] Also at Università degli Studi Guglielmo Marconi, Roma, Italy
[az] Also at Scuola Superiore Meridionale, Università di Napoli 'Federico II', Napoli, Italy
[ba] Also at Fermi National Accelerator Laboratory, Batavia, Illinois, U.S.A.
[bb] Also at Lulea University of Technology, Lulea, Sweden
[bc] Also at Laboratori Nazionali di Legnaro dell'INFN, Legnaro, Italy
[bd] Also at Consiglio Nazionale delle Ricerche — Istituto Officina dei Materiali, Perugia, Italy
[be] Also at Institut de Physique des 2 Infinis de Lyon (IP2I), Villeurbanne, France
[bf] Also at Department of Applied Physics, Faculty of Science and Technology, Universiti Kebangsaan Malaysia, Bangi, Malaysia
[bg] Also at Consejo Nacional de Ciencia y Tecnología, Mexico City, Mexico

JHEP06(2026)014

[bh] Also at INFN Sezione di Torino, Università di Torino, Torino, Italy, Università del Piemonte Orientale, Novara, Italy
[bi] Also at Trincomalee Campus, Eastern University, Sri Lanka, Nilaveli, Sri Lanka
[bj] Also at Saegis Campus, Nugegoda, Sri Lanka
[bk] Also at National and Kapodistrian University of Athens, Athens, Greece
[bl] Also at Ecole Polytechnique Fédérale Lausanne, Lausanne, Switzerland
[bm] Also at Universität Zürich, Zurich, Switzerland
[bn] Also at Stefan Meyer Institute for Subatomic Physics, Vienna, Austria
[bo] Also at Laboratoire d'Annecy-le-Vieux de Physique des Particules, IN2P3-CNRS, Annecy-le-Vieux, France
[bp] Also at Near East University, Research Center of Experimental Health Science, Mersin, Turkey
[bq] Also at Konya Technical University, Konya, Turkey
[br] Also at Izmir Bakircay University, Izmir, Turkey
[bs] Also at Adiyaman University, Adiyaman, Turkey
[bt] Also at Bozok Universitetesi Rektörlügü, Yozgat, Turkey
[bu] Also at Marmara University, Istanbul, Turkey
[bv] Also at Milli Savunma University, Istanbul, Turkey
[bw] Also at Kafkas University, Kars, Turkey
[bx] Now at Istanbul Okan University, Istanbul, Turkey
[by] Also at Hacettepe University, Ankara, Turkey
[bz] Also at Erzincan Binali Yildirim University, Erzincan, Turkey
[ca] Also at Istanbul University — Cerrahpasa, Faculty of Engineering, Istanbul, Turkey
[cb] Also at Yildiz Technical University, Istanbul, Turkey
[cc] Also at School of Physics and Astronomy, University of Southampton, Southampton, United Kingdom
[cd] Also at IPPP Durham University, Durham, United Kingdom
[ce] Also at Monash University, Faculty of Science, Clayton, Australia
[cf] Also at Università di Torino, Torino, Italy
[cg] Also at Bethel University, St. Paul, Minnesota, U.S.A.
[ch] Also at Karamanoğlu Mehmetbey University, Karaman, Turkey
[ci] Also at California Institute of Technology, Pasadena, California, U.S.A.
[cj] Also at United States Naval Academy, Annapolis, Maryland, U.S.A.
[ck] Also at Ain Shams University, Cairo, Egypt
[cl] Also at Bingol University, Bingol, Turkey
[cm] Also at Georgian Technical University, Tbilisi, Georgia
[cn] Also at Sinop University, Sinop, Turkey
[co] Also at Erciyes University, Kayseri, Turkey
[cp] Also at Horia Hulubei National Institute of Physics and Nuclear Engineering (IFIN-HH), Bucharest, Romania
[cq] Now at Another institute formerly covered by a cooperation agreement with CERN
[cr] Also at Another institute formerly covered by a cooperation agreement with CERN
[cs] Also at Texas A&M University at Qatar, Doha, Qatar
[ct] Also at Yerevan Physics Institute, Yerevan, Armenia
[cu] Also at Imperial College, London, United Kingdom
[cv] Now at Yerevan Physics Institute, Yerevan, Armenia
[cw] Also at Institute of Nuclear Physics of the Uzbekistan Academy of Sciences, Tashkent, Uzbekistan
[†] Deceased

JHEP06(2026)014